

Review

Open Access



Lithium metal stabilization for next-generation lithium-based batteries: from fundamental chemistry to advanced characterization and effective protection

Yu Yan^{1,2}, Ting Zeng¹, Sheng Liu¹, Chaozhu Shu^{1,*}, Ying Zeng^{1,*}

¹College of Materials and Chemistry & Chemical Engineering, Chengdu University of Technology, Chengdu 610059, Sichuan, China.

²Institute of Fundamental and Frontier Sciences, University of Electronic Science and Technology of China, Chengdu 611731, Sichuan, China.

*Correspondence to: Prof./Dr. Chaozhu Shu, College of Materials and Chemistry & Chemical Engineering, Chengdu University of Technology, 1# Dongsanlu, Erxianqiao, Chengdu 610059, Sichuan, China. E-mail: czshu@imr.ac.cn; Prof./Dr. Ying Zeng, College of Materials and Chemistry & Chemical Engineering, Chengdu University of Technology, 1# Dongsanlu, Erxianqiao, Chengdu 610059, Sichuan, China. E-mail: zengy@cdut.edu.cn

How to cite this article: Yan Y, Zeng T, Liu S, Shu C, Zeng Y. Lithium metal stabilization for next-generation lithium-based batteries: from fundamental chemistry to advanced characterization and effective protection. *Energy Mater* 2023;3:300002. <https://dx.doi.org/10.20517/energymater.2022.60>

Received: 30 Sep 2022 **First Decision:** 9 Nov 2022 **Revised:** 25 Nov 2022 **Accepted:** 5 Dec 2022 **Published:** 11 Jan 2023

Academic Editors: Yuping Wu, Jiazhao Wang **Copy Editor:** Fangling Lan **Production Editor:** Fangling Lan

Abstract

Lithium (Li) metal-based rechargeable batteries hold significant promise to meet the ever-increasing demands for portable electronic devices, electric vehicles and grid-scale energy storage, making them the optimal alternatives for next-generation secondary batteries. Nevertheless, Li metal anodes currently suffer from major drawbacks, including safety concerns, capacity decay and lifespan degradation, which arise from uncontrollable dendrite growth, notorious side reactions and infinite volume variation, thereby limiting their current practical application. Numerous critical endeavors from different perspectives have been dedicated to developing highly stable Li metal anodes. Herein, a comprehensive overview of Li metal anodes regarding fundamental mechanisms, scientific challenges, characterization techniques, theoretical investigations and advanced strategies is systematically presented. First, the basic working principles of Li metal-based batteries are introduced. Specific attention is then paid to the fundamental understanding of and challenges facing Li metal anodes. Accordingly, advanced characterization approaches and theoretical computations are introduced to understand the fundamental mechanisms of dendrite growth and parasitic reactions. Recent key progress in Li anode protection is then



© The Author(s) 2023. **Open Access** This article is licensed under a Creative Commons Attribution 4.0 International License (<https://creativecommons.org/licenses/by/4.0/>), which permits unrestricted use, sharing, adaptation, distribution and reproduction in any medium or format, for any purpose, even commercially, as long as you give appropriate credit to the original author(s) and the source, provide a link to the Creative Commons license, and indicate if changes were made.



comprehensively summarized and categorized to generate an overview of the respective superiorities and limitations of the various strategies. Furthermore, this review concludes the remaining obstacles and potential research directions for inspiring the innovation of Li metal anodes and endeavors to accomplish the practical application of next-generation Li-based batteries.

Keywords: Next-generation batteries, Li metal anodes, high energy density, advanced protection strategy, practical application

INTRODUCTION

Possessing a number of desirable features, including high round-trip efficiency, long cycling life, flexible power and energy characteristics to meet different grid functions, pollution-free operation and low maintenance, state-of-the-art commercial lithium-ion batteries (LIBs) based on the rocking chair concept have produced spectacular advances in transportation and communication diversification since their introduction in the early 1990s^[1,2]. Unfortunately, this type of electrical energy storage device cannot keep pace with the progress in the cutting-edge electronics industry^[3]. By its nature, the working principle of LIBs is based on the intercalation of Li⁺ ions into layered electrode materials, such as graphite anodes and Li metal oxide cathodes, leading to the fact that Li⁺ ions can only be intercalated topotactically into certain specific sites. The drawback of capacity limitation (372 mAh g⁻¹) for the aforementioned conventional anodes can no longer meet the rapidly growing demands for power and energy density (the theoretical energy density of LIBs is typically limited to 420 Wh kg⁻¹ or 1400 Wh L⁻¹), which stimulates the pursuit of alternative anodes with high energy density^[4]. With an extremely high theoretical specific capacity (3860 mAh g⁻¹) and the most negative electrochemical potential (-3.040 V vs. a standard hydrogen electrode), Li metal is strongly deemed as the ultimate anode for secondary batteries [Figure 1A and B]^[5]. Different from intercalation chemistry, Li metal batteries (LMBs), such as lithium-oxygen (Li-O₂) and lithium-sulfur (Li-S) batteries, operate based on metal plating and stripping at the Li anode side and conversion reactions at the cathode side. The non-topotactic nature of these reactions endows Li-O₂ batteries (3505 Wh Kg⁻¹) and Li-S batteries (2600 Wh Kg⁻¹) with high theoretical energy density, thereby making them become the optimal choices for next-generation secondary batteries.

In fact, Li metal anodes were employed in the infancy of Li battery research, including the assembly of primary Li cells in digital watches, calculators and implantable medical devices by Whittingham at Exxon in the 1970s^[5,6]. Nevertheless, these non-rechargeable primary batteries led to serious waste, high costs and environmental pollution. In the 1980s, the first generation of commercially rechargeable LMBs, assembled with an excess amount of Li, was proposed by Moli Energy^[7]. However, due to the intrinsic chemical and electrochemical activity of Li, the use of Li metal anodes triggers a series of notorious dilemmas during the charge/discharge processes, including dendrite formation and growth, Li corrosion, the formation of dead Li, unstable solid electrolyte interfaces (SEI) and volume expansion, yielding fatal short circuits, severe lifespan attenuation and capacity loss in LMBs. Safety concerns, including inflammation and even explosion, resulting from the short circuit of batteries, render the recall of all the cells, ultimately making LMBs noncompetitive in the commercial market. In subsequent years, the progress regarding Li metal anodes has been limited. In particular, with the first LIBs commercialized by Sony Corporation in the 1990s, the commercialization of Li metal anodes was almost completely halted. Nowadays, the energy density limitation of traditional LIBs based on graphite anodes has brought about a gradual revival of LMBs and there has been a recent global blooming in terms of the number of publications [Figure 1C] and citations [Figure 1D] in designing batteries where Li metal is used as the anode. Based on data from the Web of Science, more than 500 publications dealing with the above challenges have been published from 2014 to 2016. Remarkably, an average of 15 articles have come out per month since 2016, indicating a roaring expansion in this field.

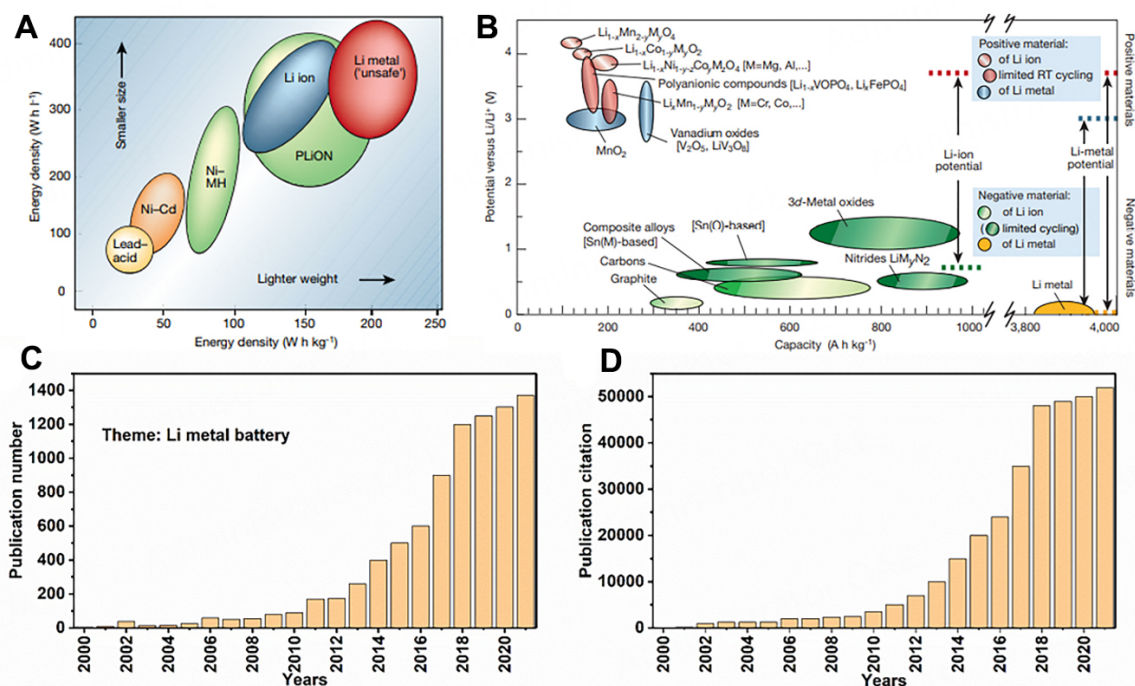


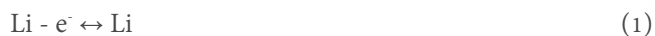
Figure 1. (A) Volumetric and gravimetric energy density comparison of different battery technologies. (B) Voltage versus capacity of positive and negative electrode materials. Reprinted with permission from Ref.^[3]. Copyright (2019) Springer Nature. Number of (C) publications and (D) citations related to "lithium metal anodes" up to November 2021. Data were on from the Web of Science.

In this review, the growing research efforts regarding the application of Li metal anodes in LMBs are discussed. This review begins with an introduction to the fundamental chemistry of Li metal and the enormous challenges that impede the development of Li metal anodes. The details of the various techniques employed to characterize the degradation of Li electrodes in batteries are then summarized with an emphasis on advanced *in situ* electrochemistry analysis. Furthermore, some theoretical simulation and calculation methods are overviewed to strengthen the insights into the Li deposition behavior. The recent key progress in developing practical Li electrodes is summarized and mainly divided into four categories: (1) modulating the anode structure to regulate the electron/Li⁺ ion conductive behavior on the anode surface via electron-conductive, ionic-conductive and mixed ion and electron-conductive host materials; (2) modifying the anode/electrolyte interface to reshape the Li⁺ ions flux and mechanically block the dendrites by establishing an external barrier; (3) optimizing the electrolyte composition to adjust Li⁺ solvation in the electrolyte; and (4) designing the membrane to detect the dendrites and suppress the final cell short circuit. Eventually, further developments in the design strategies of advanced Li metal anodes for stable LMBs are presented. This review raises key advances and outlines future strategies for next-generation high-energy storage systems.

LI METAL CHEMISTRY

Intrinsic properties of Li metal anodes

Li metal possesses the smallest radius of all metal atoms and the lowest density (0.534 g cm⁻³) of alkali metals, thereby endowing it with ultrahigh storage capacity. The theoretical specific capacity (Q_c) of Li can be calculated based on the following equations, with an ultrahigh Q_c of 3860 mAh g⁻¹ obtained^[8]:



$$Q_c = \frac{\text{charge}}{\text{mass}} = \frac{6.02 \times 10^{23} \text{ atom} (1.6 \times 10^{-19} \frac{\text{C}}{\text{atom}}) \frac{1 \text{ mAh}}{3.6 \text{ C}}}{1 \text{ mol} \frac{6.94 \text{ g}}{\text{mol}}} = 3.86 \times 10^3 \text{ mAh g}^{-1} \quad (2)$$

As an electrode, Li has the most negative electrochemical potential (-3.040 V vs. a standard hydrogen electrode) among all anodes, which endows LMBs with high discharge voltage and energy density. Furthermore, Li metal anodes are able to provide an energy-dense Li-ion source, which enables the anode to be compatible with extensive cathode materials, including non-lithiated cathodes, leading to the versatility of battery design. For LMBs, the electrochemical deposition/dissolution of Li metal takes place on the anodic side. Simultaneously, Li⁺ ions are consumed/accumulated at the cathodic side. According to the paired cathode materials (e.g., intercalation cathode materials, O₂ and S), LMBs can be divided into three primary categories, namely, lithium-lithium intercalation compound, Li-O₂ and Li-S batteries. The reaction principle of LMBs during the charge/discharge processes is described as follows^[9-11]:

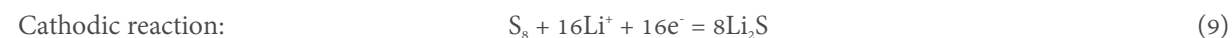
Lithium-lithium intercalation compound batteries (taking Li_{1-x}MO₂ as an example):



Li-O₂ battery:



Li-S battery:



Challenges facing Li metal anodes

Despite the tremendous potential of next-generation secondary battery applications, the Li anode still faces a multitude of challenges to overcome: (i) electrolyte depletion due to the continuous reaction with Li metal and mechanical instability of the SEI layer; (ii) dendrite formation deriving from initial uneven Li nucleation and the subsequent selective deposition; and (iii) infinite relative volume change. These shortcomings inevitably lead to unsatisfactory Coulombic efficiency (CE), short lifetimes and even safety problems, such as thermal runaway and explosion hazards.

Unstable formation of SEIs on Li surface

The SEI has become a critical research topic since the pioneering work of Aurbach and Peled^[12-15]. Different models, including mosaics (polyhetero microphase), vacancies (Schottky lattice defects), double-layer capacitors, multilayers and monolithic SEIs, can be used to explain the chemical and physical properties of SEIs [Figure 2A-E]^[12,13,16,17]. Among them, the mosaic model with various components and a dual-layer architecture is commonly accepted. The inner layer, which is close to the anode, consists of species with low oxidation states, including LiF, Li₃N, Li₂O, Li₂CO₃ and LiOH, and is labeled as an inorganic layer. In contrast, the outer layer of the SEI is composed of species with high oxidation states, such as RCOO₂Li, RO₂Li and ROCO₂Li, and is labeled as the organic layer.

Due to the significantly negative electrochemical potential of Li⁺/Li, virtually any available electrolyte can be reduced by Li metal to form electrically insulating and ionically conductive species on the electrode surface [Figure 3A]. Goodenough *et al.* explained the SEI formation mechanism based on the frontier molecular orbital theory^[18]. As shown in Figure 3B, μ_A and μ_C refer to the electrochemical potentials of the anode and cathode, respectively. Accordingly, E_{LUMO} and E_{HOMO} are representative of the voltage that corresponds to the lowest unoccupied molecular orbital (LUMO) and highest occupied molecular orbital (HOMO) of the electrolytes, respectively. If $\mu_A > E_{LUMO}$, electrons tend to transfer from the anode surface to the unoccupied orbital of the electrolyte, triggering the reduction reaction of the electrolyte. The generated SEI serves as a barrier, preventing further decomposition of the electrolyte. Analogously, redox reactions facilitate the formation of the SEI between the electrode and electrolyte in the case of $\mu_C < E_{HOMO}$.

The component and structure of the SEI film are strongly dependent on the composition of the electrolyte, mainly organic carbonate- and ether-based electrolytes, which determine the primary properties of the SEI film. Organic carbonates are the most commonly used electrolyte solvents for LMBs. The preliminary composition of the SEI in a carbonate-based electrolyte system is mainly made up of Li alkyl carbonates (ROCOOLi, where R is an organic group related to the solvent), which are generated by the one-electron reduction of organic carbonates^[14]. More stable components of Li₂CO₃, Li₂O and Li halides can be presented in the SEI depending on the used salts^[15]. However, the SEIs formed in organic carbonate-based electrolytes lack flexibility, which makes them susceptible to interfacial fluctuations. With significant dendrite suppression capacity, ethers are considered as strong candidates for electrolyte solvents for LMBs in multiple systems, which can be ascribed to the formation of oligomers with strong affinity to the Li surface and excellent flexibility^[19]. For example, 1,3-dioxolane (DOL), as a widely used ether solvent in LMBs, can form oligomeric SEI films with superior flexibility and strong binding affinity to Li metal. As the Li metal anode is cycled in the DOL-based electrolyte, DOL is reduced on the Li metal surface to form different alkoxy species, leading to its anionic partial polymerization to form LiO-(CH₂CH₂OCH₂O)_nLi type species. A surface film is thus formed by these short-chain oligomers of poly(ethylene oxide) that is elastomeric and can accommodate the morphological change of the anode surface upon long-term cycling.

The SEI film is an essential path for the desolvation and reduction of Li⁺ ions on the electrode, where the diffusion behavior of Li⁺ ions crucially affects the Li deposition morphology. Specifically, once solvated Li⁺ ions are transported to the SEI surface under the electric field, the SEI is capable of desolvating Li⁺ ions and the naked Li⁺ ions are then transported to the current collector where they are reduced. Furthermore, robust and dense SEI can prevent Li exposure, which directly causes the Li corrosion. A desired SEI for efficient and safe LMBs should possess the following features: (1) excellently ionic conductivity; (2) proper thickness, which is sufficient to prevent electron penetration to electrolyte completely and appropriate for the diffusion resistance of Li⁺ ions; (3) extraordinary chemical and electrochemical stability in composition

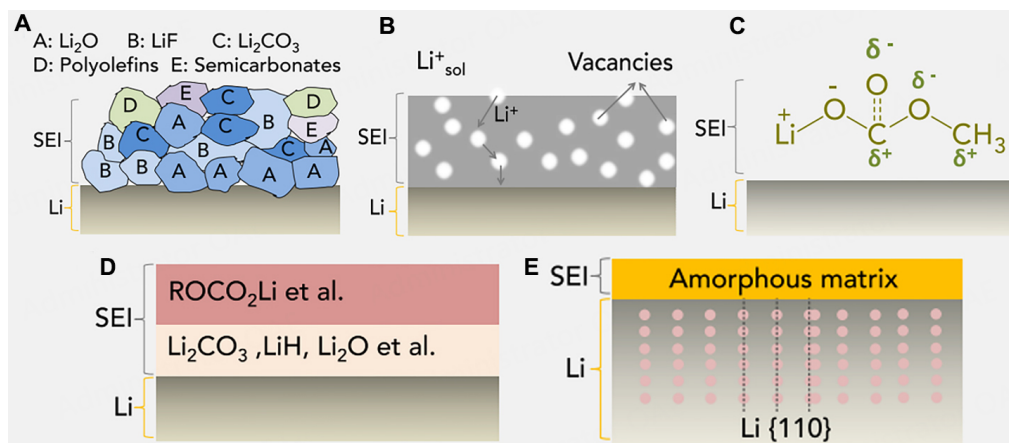


Figure 2. Schematic illustrations of various SEI models: (A) mosaics (polyhetero microphase); (B) vacancies (Schottky lattice defects); (C) double-layer capacitors; (D) multilayers; (E) monolithic SEI. Reprinted with permission from Ref. [126]. Copyright (2021) Cell Press.

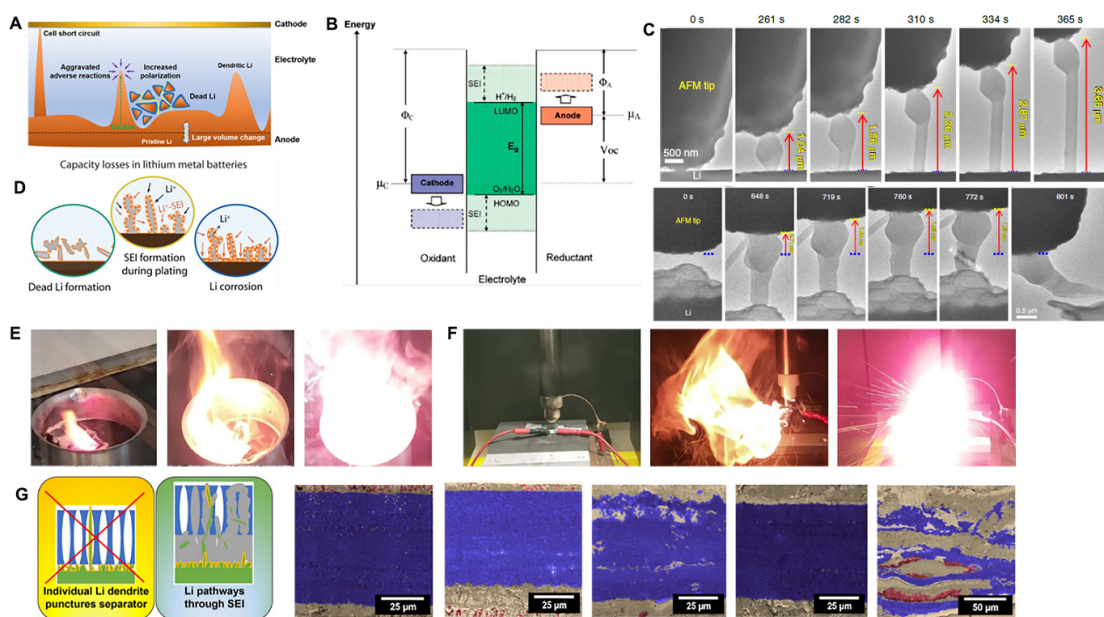


Figure 3. (A) Schematic illustration of challenges facing Li metal anodes. (B) SEI formation conditions in a liquid electrolyte. Reprinted with permission from Ref. [8]. Copyright (2017) American Chemical Society. (C) Time-lapse TEM images of Li whisker growth. Reprinted with permission from Ref. [22]. Copyright (2020) Springer Nature. (D) Schematic representation of dead Li including Li⁺ ions in SEI formation and Li metal wrapped by insulating byproducts. Reprinted with permission from Ref. [92]. Copyright (2020) American Chemical Society. (E) Fire and (F) explosion phenomena of Li metal anode. Reprinted with permission from Ref. [38]. Copyright (2020) Springer Nature. (G) Schematic diagram and scanning electron micrographs of high-rate cycled angled sections showing failure within two stacked Celgard 2325 separators. Reprinted with permission from Ref. [39]. Copyright (2021) American Chemical Society.

during long-term cycling; and (4) excellent mechanical properties to adapt the volume variation of Li during repeated charge/discharge processes.

Li dendrite and relative issues

During electrodeposition, the growth of metal “dendrites” is a common phenomenon. Many metals, such as Zn, Cu, Ag, Sn and so on, were found to exhibit ramified morphologies under given electrodeposition conditions [20,21]. Generally, metallic electrodeposition can be divided into two stages: early nucleation and late deposition [Figure 3C] [22]. During the deposition process, a critical thermodynamic radius needs to be

reached to favor dendrite formation energetically and a critical kinetic radius is required to keep the isolated embryo growing. As the growth continues, localized electric fields dominate the morphology of the Li deposits in the late growth regime to form dendrites with prolonged length and sometimes augmented diameter.

To explain the propagation of dendrites during the electrochemical deposition of metals, various models have been proposed: (i) surface tension model; (ii) diffusion-limited model; and (iii) electromigration-limited model^[23]. Barton *et al.* comprehensively proposed the surface tension model in which surface tension between the electrolyte and metal was considered to be one of the driving forces for Li dendrite growth^[24]. At the initial stage, the electrodeposition of metal ions on an elevated region of the anode surface with spherical diffusion was faster than that on a flat surface with the linear diffusion, leading to preliminary protrusions with enhanced diffusion conditions^[24-26]. Later, the possible Li morphology could be estimated via a fluid dynamics mathematical model and it was confirmed that particle-shaped Li deposition would deform Li dendrites under high surface tension^[27]. In the classical diffusion-limited model, metal ions move randomly and reach active sites of the electrode where the deposition probability of mobile ions can be defined as a balance between the rate of the electrochemical reaction and the bulk diffusion^[28]. The diffusion becomes dominant rather than the reductive deposition while a deposition probability is low, leading to the suppression of dendrite formation. In contrast, the high deposition probability always causes the ramified dendrite structure. The model was applied to simulate the reductive deposition of Li⁺ ions and found that the formation of dendrites was related to the competition between the diffusion of Li⁺ ions in the SEI film and the interfacial deposition reaction^[29]. Moreover, dendrite propagation can be successfully inhibited by pulse charging conditions, which altered the electrodeposition morphology of various metals, thus effectively suppressing dendrite growth^[30].

In the Chazalviel model, dendrite initiation was described to be limited by the electromigration process rather than the diffusion process^[20]. It was demonstrated that the current density can change the ion concentration gradient, i.e., the lower current density maintains a stationary ion distribution without propagation of Li dendrite, while the higher current density introduces the depletion of cations and anions at the electrode interface and the resulting local space charge field leads to the growth of dendritic Li. The critical current density, J^* , was defined as the boundary behavior between the high and low current densities as follows:

$$J^* = \frac{2eC_0D}{t_aL} \quad (10)$$

where e represents the electronic charge, C_0 represents the initial concentration of the electrolyte, D represents the ambipolar diffusion coefficient, t_a represents the transport number of anions and L represents the distance between the electrodes. In particular, the nuclei of Li dendrites were formed when the concentration of ions near the electrode dropped to zero. The time of the concentration of ions dropping to zero was defined as Sand's time, τ_{sand} . Furthermore, the corresponding current density was labeled as the limiting current density when the ion concentration approached zero.

In the 1990s, Chazalviel's space charge model was verified and supplemented^[31,32]. In particular, to explain the Li dendrite formation and growth even at a low current density below J^* , the heterogeneity of the electrode surface was considered in the model based on the fact that the variation in local current density could be caused by the inhomogeneous microstructures of the electrode surface^[33]. Severe Li dendrite growth usually produces a large number of derivative problems, such as dead Li (i.e., Li losing contact with

the electrode surface and can no longer participate in the electrode reactions) [Figure 3D]. The formation of dead Li indicates an irreversible loss of battery capacity^[34]. Both uncontrollable dendritic Li growth and dead Li are believed to be the reason for the low CE (less than < 99%) of Li deposition/dissolution in nonaqueous electrolytes^[35]. In addition to the formation of dead Li, the newly exposed Li dendrites on the surface can be rapidly corroded by the nonaqueous electrolyte, leading to the formation of a thick SEI with poor conductivity. Due to the repeated generation/fracture of the unstable SEI during charge/discharge processes, the exposed fresh Li reacts with the electrolyte continuously. Electrolyte depletion and electrochemical corrosion of Li metal eventually lead to low CE and capacity decay^[36,37]. Among the above-discussed issues triggered by dendritic growth, safety concerns, including battery fires [Figure 3E] and even explosion hazards [Figure 3F], which result from short circuit risks [Figure 3G], are also top priorities for developing practical LMBs^[38,39].

Infinite relative volume change

Unlike insertion type anode materials (such as C, Si, Al, Ge and Sn), metallic Li is the conversion type anode with an enormous volume change, far exceeding those of intercalated anodes, such as graphite (with the volume change of 10%) and silicon (with the volume change of 400%) during each plating/stripping process^[40]. The accommodative rate of the SEI cannot easily keep up with the expansion/contraction of the anode during the plating/stripping of Li, eventually leading to damage to the SEI and dendrite growth. This volume change can also induce the destruction of the electrode and electrolyte interfaces, resulting in a decay in electrochemical performance. Actually, the pulverized and insulting LiH has been proposed as one of the reasons for anode expansion of LMBs, which is formed by the parasitic reaction between Li metal and H₂ in batteries^[41]. Lu *et al.* found that at a current density of 1.5 mA cm⁻², no evidence of separator penetration by dendritic Li could be found in the failed battery. Instead, expansive regions of Li/electrolyte interface inhibited the contact among Li grains, leading to a porous and loose structure^[42]. The increased resistance of this porous interphase was believed to be the true cause of the eventual battery failure. Moreover, from a practical perspective, an areal capacity of at least 3 mAh cm⁻² is required for a single-sided commercial electrode, which corresponds to a relative thickness change of ~14.6 μm for lithium. For future batteries, this value might be even higher, which means that the movement of the Li interface may reach tens of microns during cycling, which imposes a serious challenge on the stability performance of the SEI.

CHARACTERIZATION OF LI METAL ANODES

There are a variety of detection and characterization techniques used to study the Li metal anode. Since Li is extremely reactive, *ex situ* techniques often require very careful sample preparation and handling to minimize damage to the electrode. Conversely, as typically nondestructive techniques, *in situ* techniques are conducted with a cell in its fully assembled condition, thus furnishing dynamic cell information in non-equilibrium states. In the past several years, there has been a rapid increase in research interest in *in situ* technologies, including *in situ* morphology and composition characterization, to continuously capture transient metastable information on Li metal anodes as a function of time.

Morphological and microstructural characterization of Li surface

In situ imaging techniques, including *in situ* optical image techniques, electron-based analysis, scanning probe-based tools, X-ray and synchrotron-based analysis, magnetism-based techniques, neutron-based analysis and other *in situ* techniques, have been widely applied to qualitatively study the composition of Li-containing species^[43-46]. Optical image and microscopy technologies are based on the light wave of the object being reflected and projected by the detector to form the image. Therefore, optical microscopy (OM) in conjunction with an *in situ* reaction cell and electrochemical workstation is the most widely used image observation equipment. More importantly, it is the most direct, rapid, feasible and low-cost method to

analyze the deposition and dissolution behavior of Li metal. In 1998, Osaka *et al.* employed *in situ* OM to explore the effect of the electrolyte on the Li deposition morphology and anode cycling efficiency^[47]. Arakawa *et al.* investigated the relationship between dead Li formation and the Li plating morphology by recording the film attached to an optical microscope to obtain photographs^[34]. Subsequently, Yamaki *et al.* employed *in situ* OM to probe the internal mechanism of deposition and dissolution of Li metal in LiClO₄-PC and proposed the famous whisker model based on a mathematical analysis showing that dendritic Li may grow from the current collector during deposition^[27]. Inevitably, stress from the bottom regions can seriously destroy the SEI interphase, enabling Li whiskers to continuously grow in the form of extrusion. Nevertheless, Steiger *et al.* proposed a different view of Li cycling behavior in a LiPF₆-EC/DMC electrolyte^[48]. They claimed that crystal defects control the Li deposition behavior, i.e., newly fresh Li atoms are electrodeposited to the defective regions. In addition to defects, Li metal can also grow from grain boundaries, kinks and chemical inhomogeneities, such as contaminants. Furthermore, they proved that dendritic growth is based on the defect-controlled deposition mechanism, challenging the conventional mechanism based on ion transport^[49]. Moreover, Shen *et al.* studied the impacts of current density, magnetic field and electromigration on dendritic Li growth via *in situ* OM observation^[50-52]. Although *in situ* OM has shown its effectiveness in observing dendrite growth and battery failure, it still possesses some drawbacks, the most important of which are the low resolution and poor image clarity in complicated electrolyte circumstances^[53].

Due to higher spatial resolution than *in situ* OM, *in situ* scanning electron microscopy (SEM) has been widely applied to battery research. Krauskopf *et al.* investigated the Li growth kinetics on a garnet-type solid-state electrolyte (SSE) at the microscale via *in situ* SEM^[54]. Motoyama *et al.* used *in situ* SEM to observe the plating and stripping behavior of Li metal in a LiPON electrolyte^[55]. As shown in [Figure 4A](#), a Li island grows laterally over time without damaging the wolfram film. During the Li dissolution process, the dome top of the island first begins to shrink and then the lateral bulges reduce gradually. *In situ* electrochemical SEM (EC-SEM) provides a powerful tool to reveal the reaction mechanism in electrochemical systems. For instance, Rong *et al.* found that the addition of single LiNO₃ in a LiTFSI-DOL/DME electrolyte could hardly inhibit the Li dendrite formation and growth via EC-SEM^[56].

As an advanced technology, *in situ* transmission electron microscopy (TEM) has been developed gradually. With high energy electrons as the excitation source, the operation principle of *in situ* TEM is similar to that of *in situ* SEM, but its spatial resolution is higher than *in situ* SEM. Furthermore, TEM can provide chemical and structural information for electrodes at the nanoscale^[57]. Initially, Huang *et al.* reported an “open” *in situ* TEM cell^[58]. However, “open” TEM inevitably has its own defects: (1) the electrode is in point contact with the electrolyte, and thus the mode of Li⁺ ion diffusion is quite distinct from the actual cell; (2) the strong electron beams are detrimental to some polymer electrolytes; and (3) some SSEs can cause additional overpotential. A “closed” cell with a chamber was then designed to seal off the liquid electrolyte [[Figure 4B](#)] to avoid the effect of the high vacuum on the system^[59]. Moreover, clear dynamic information regarding Li stripping/plating processes can be obtained using high-angle annular dark field scanning transmission electron microscopy (HAADF-STEM)^[60]. Gong *et al.* employed operando HAADF-STEM to study Li electrodeposition and dissolution, which explained the F-enriched interface formation on Li deposits^[61]. For the past few years, Li *et al.* upgraded Li dendrite images at the atomic scale via cryogenic-electron microscopy technology (cryo-EM) [[Figure 4C and D](#)]^[62]. Wang *et al.* observed the phase transition of ordered (crystalline) Li and disordered (glassy) Li via cryo-TEM, revealing the transient structural evolution during Li deposition^[63].

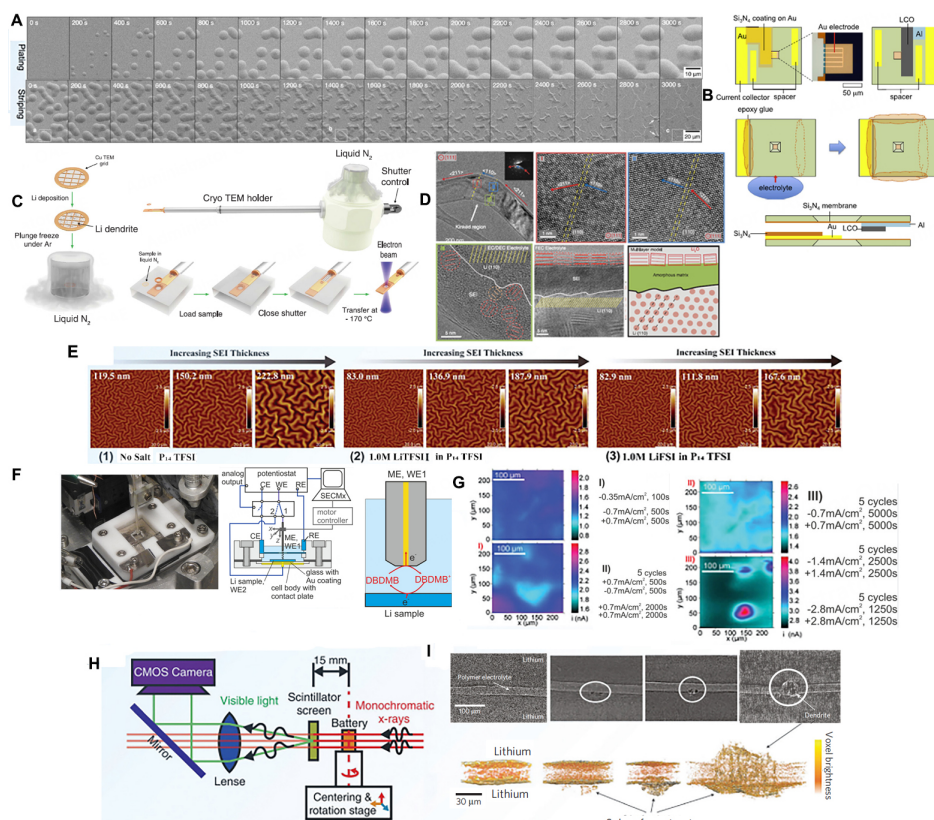


Figure 4. (A) Sequential SEM images during Li electrodeposition/dissolution processes based on a wolfram film with a thickness of 90 nm and a LiPON electrolyte at $50 \mu\text{A cm}^{-2}$. (B) Schematic illustration of liquid confining cell. Reprinted with permission from Ref.^[59]. Copyright (2017) Elsevier. (C) Preserving and stabilizing Li by cryo-EM. (D) Atomic-resolution TEM images of Li metal and SEI. Reprinted with permission from Ref.^[62]. Copyright (2017) American Association for the Advancement of Science. (E) AFM (two-dimensional, 2D) images of buckled surface topography from three RTIL electrolytes: no-salt P_{14} TFSI; 1.0 M Li TFSI in P_{14} TFSI; 1.0 M Li FSI in P_{14} TFSI. Reprinted with permission from Ref.^[66]. Copyright (2018) American Chemical Society. (F) SECM cell for battery electrodes including photograph, cross-sectional schematic, reactions at the microelectrode (ME) and sample during imaging (ME radius and ME-sample distance are enlarged for clarity). (G) Sequence of SECM feedback images recorded at different charge/discharge processes. Reprinted with permission from Ref.^[67]. Copyright (2020) Wiley-VCH. (H) Sketch of X-ray tomography setup. Reprinted with permission from Ref.^[70]. Copyright (2013) American Association for the Advancement of Science. (I) X-ray tomography slices showing cross sections of symmetric lithium cells cycled to various stages and magnified 3D reconstructed volumes of cells. Reprinted with permission from Ref.^[71]. Copyright (2014) Springer Nature.

In situ atomic force microscopy (AFM) has also been generally applied to obtaining surface information, such as the analysis of the morphology of deposits and exploration of the Young's modulus, which cannot be detected by other microscopy techniques. Aurbach *et al.* studied the impact of the electrolyte component on Li deposition behavior at low and high current densities via *in situ* AFM observation^[64]. Subsequently, Kitta *et al.* employed *in situ* AFM combined with adhesion mapping to confirm that fresh Li protrusion possessed a thinner SEI film and lower adhesion might grow rapidly^[65]. Yoon *et al.* used *in situ* AFM to detect the plane strain modulus of an SEI that was formed in an ionic liquid at room temperature through a mechanical analysis method^[66]. As exhibited in Figure 4E, under compressive stress, the SEI layer generates surface buckling. According to the calculated results, the strain modulus of the SEI film for all the samples ranges from 1.2 to 2.0 GPa. Based on an electrochemical reaction, scanning electrochemical microscopy (SECM) is a kind of scanning technology that uses a small driving probe to scan samples and obtains corresponding electrochemical information. The interfaces between measured liquid and solid samples, which can be insulators, semiconductors and conductors, are effectively monitored, enabling SECM to timely obtain the current on the electrode. Krueger *et al.* investigated the current evolution of the selected

SEI region via an *in situ* SECM device [Figure 4F]^[67]. As shown in Figure 4G, it can be found that the gap between the minimum and maximum currents gradually increases with the enhancement of applied current during cycling. The SEI will be increasingly challenged by the heavy current due to the continually changing surface shape of metallic Li in the subsequent cycles; thus, it can be applied to detect the appearance of lithium protrusions. Furthermore, laser scanning confocal microscopy (LSCM) and scanning tunnelling microscopy (STM) have also been exploited to investigate Li metal anodes^[68].

In situ X-ray imaging technologies, such as transmission X-ray microscopy (TXM) and X-ray tomography (XRT), can establish real-time three-dimensional (3D) images of Li deposits without damaging cells. Considering the high energy of X-rays, TXM can be employed to study thick samples. Using *in situ* TXM, Cheng *et al.* first revealed the dynamics of dendritic Li growth in 1 M LiPF₆-ethylene carbonate (EC)/diethyl carbonate (DEC)^[69]. Notably, as a brand-new 3D detection technology, XRT is capable of investigating the inner electrode structure without slicing treatment. It photographs electrodes from different angles by rotating samples and then reconstructs 3D images through remodeling [Figure 4H]^[70]. Harry *et al.* reported that dendritic Li was mainly distributed inside the electrode at the initial stage, i.e., below the interface of the electrode/polymer electrolyte^[71,72]. Crystal impurities and the subsurface structure are the nucleation seeds of Li dendrites. Subsequently, Li branches pierce the electrolyte and reach the cathode side, eventually leading to short circuit of the battery [Figure 4I]. Yu *et al.* systematically estimated the impact of various electrolyte systems on the plating and stripping processes of Li metal via synchrotron-based X-ray imaging technology^[45]. They proposed that the excessive overpotential generated a higher nucleation density, leading to smaller nuclei during the charge process, which is consistent with the previously reported result^[73].

In situ nuclear magnetic resonance (NMR) is commonly used to monitor the component variation of the electrolyte, electrode and interface. As a noninvasive imaging technique developed from *in situ* NMR, *in situ* nuclear magnetic resonance imaging (MRI) can achieve sufficient temporal and spatial resolution of the ⁷Li chemical shift. Ilott *et al.* reported the utilization of indirect MRI with 3D imaging to investigate the microscopic structure of Li metal, showing that dendritic growth was distorted rather than unidirectional until the short circuit was formed^[74]. Because this method not depending on measuring Li directly, it is also suitable for several metallic dendrites, such as sodium, zinc and magnesium anodes. *In situ* electron paramagnetic resonance (EPR), in which the unpaired electron spins rather than nuclear spins are present in EPR when applying a magnetic field, is an emerging technique in Li metal anode research. Sathiya *et al.* first observed uneven Li deposition with a LiPF₆-EC/PC/DMC electrolyte in a Li₂Ru_{0.75}Sn_{0.25}O₃/Li battery by *in situ* EPR^[75]. Wandt *et al.* found that the formation of microstructured (mossy/dendritic) Li was greatly reduced after the addition of FEC via *in situ* EPR and *ex situ* SEM^[76].

Neutron radiography and tomography (NR/NT), whose imaging principles are based on the neutron absorption gradient determined by the permeability and absorption of sample composition and density, are typical 2D and 3D imaging technologies, respectively. Recently, Song *et al.* investigated the distribution and growth mechanism of Li dendrites by *in situ* NR/NT techniques^[77]. Combined with electrochemical tests, it was confirmed that the dendritic Li growth between the anode and LiMn₂O₄ contributed to the short circuit. Sun *et al.* used *in situ* NT combined with *in situ* XRT to demonstrate the relationship between the overall electrochemical performance of a Li-O₂ battery and the evolution of Li morphology, which fully revealed that the irreversible conversion of Li metal from the bulk structure to porous state^[78]. This work has advanced the mechanism of battery failure, which contributes to new insights into future battery design.

Chemical composition and bonding analysis of SEI components

A number of methods have been developed to investigate the evolution of the electrode/electrolyte interface during cycling. Li detection and quantification can be acquired by *in situ* X-ray diffraction (XRD), Raman spectroscopy, Fourier transform infrared (FTIR) spectroscopy, NMR, MRI and neutron depth profiling (NDP) analysis. The composition of the surface reaction products can be revealed by *in situ* X-ray photoelectron spectroscopy (XPS) and cryo-TEM analysis. The salt and Li-ion concentration gradients can be investigated by holographic interferometry, *in situ* stimulated Raman scattering (SRS) microscopy and MRI analysis. *In situ* XRD [Figure 5A] provides a range of signals, such as some metastable information that cannot be obtained through *ex situ* XRD^[79]. Shen *et al.* proved the excellent stability of a LiF-modified Li anode in the 1 M LiPF₆/EC/DEC electrolyte by *in situ* XRD^[80]. As shown in Figure 5B, at the first cycle, the electrolyte in the battery system based on bare Li anode is decomposed to the formation of the SEI film and Li dendrites. However, the diffraction peak change in the battery system based on the LiF-modified Li electrode is negligible, indicating the stable SEI.

In situ Raman measurements [Figure 5C] have advantages over *in situ* XRD due to their applicability to analyze poorly crystalline and amorphous compounds^[81]. Furthermore, Raman spectroscopy is feasible for studying the electrolyte, electrode and interface. Qiu *et al.* found that minute amounts of O₂ in Li-O₂ batteries can react rapidly with metallic Li to generate an SEI enriched with Li₂O, Li₂O₂ and LiOH species, which protect the anode from further reacting with salts and solvents^[82]. The inhomogeneity of the interfacial Li-ion concentration is closely related to the dendritic Li growth; hence, significant studies have been devoted to the concentration variation of Li⁺ ions at the electrode/electrolyte interface. For example, by using *in situ* Raman spectroscopy measurements, Chen *et al.* found a Raman band at 741.8 cm⁻¹, which was attributed to the S-N stretching and coupled CF₃ bending in TFSI, proving the uniform distribution of Li⁺ ions in the MIP-based electrolyte [Figure 5D]^[83]. In addition, as a non-linear Raman technique, SRS has been successfully applied to investigate the variation of the interfacial Li⁺ ion concentration, realizing the 3D visualization of ion depletion and the corresponding dendrite growth^[84]. Due to the high measurement accuracy, rapid measurement speed, high resolution and detection sensitivity, *in situ* FTIR spectroscopy has been used to track electrolyte decomposition and SEI construction. According to *in situ* FTIR results, Hu *et al.* discovered that nitrile compounds are attractive electrolyte candidates with wide electrochemical windows, outstanding thermal stability and high safety at high voltages^[85,86]. However, nitrile compounds are highly corrosive to Li metal. XPS, which is usually used to characterize the electronic structure of surface elements and local chemical environments, is an effective means for investigating solid surfaces. Schwöbel *et al.* first reported the SEI layer between metallic Li and LiPON using *in situ* XPS^[87]. A more fundamental study of the reaction of the active metallic Li with the atmosphere was carried out by exposing Li to CO₂ by Etzbarria *et al.*^[88]. Yan *et al.* investigated the influence of the FEC on the SEI constituents by sputtering XPS, via which it was revealed that the SEI consisted of a dense two-layer structure with the bottom layer composed of inorganic species, such as Li₂CO₃ and LiF, and the bottom layer composed of organic species, such as ROCO₂Li and ROLi^[89].

In situ NMR can be used to realize the quantitative evaluation of various Li morphologies because the radiofrequency can completely penetrate the Li microstructure [Figure 5E]^[90-92]. According to the reported results, the position variation of the Li microstructure could be detected by the changed signal^[93]. The resonance displacement of NMR shifts with various metallic Li structures, such as the characteristic peaks of dendritic Li and mossy Li at 270 and 261 ppm, respectively [Figure 5F]^[94]. In addition, the intensity of NMR varies with the amount of Li deposits. This difference in peak position and intensity enables the deposited Li to be quantitatively evaluated. For instance, Gunnarsdóttir *et al.* calculated the amount of “dead Li” from the NMR spectra in Figure 5G and H^[92]. In addition, 3D matrix images on the timescale of an electrochemical reaction can be generated by specific chemical shift points, which allows *in situ* MRI to

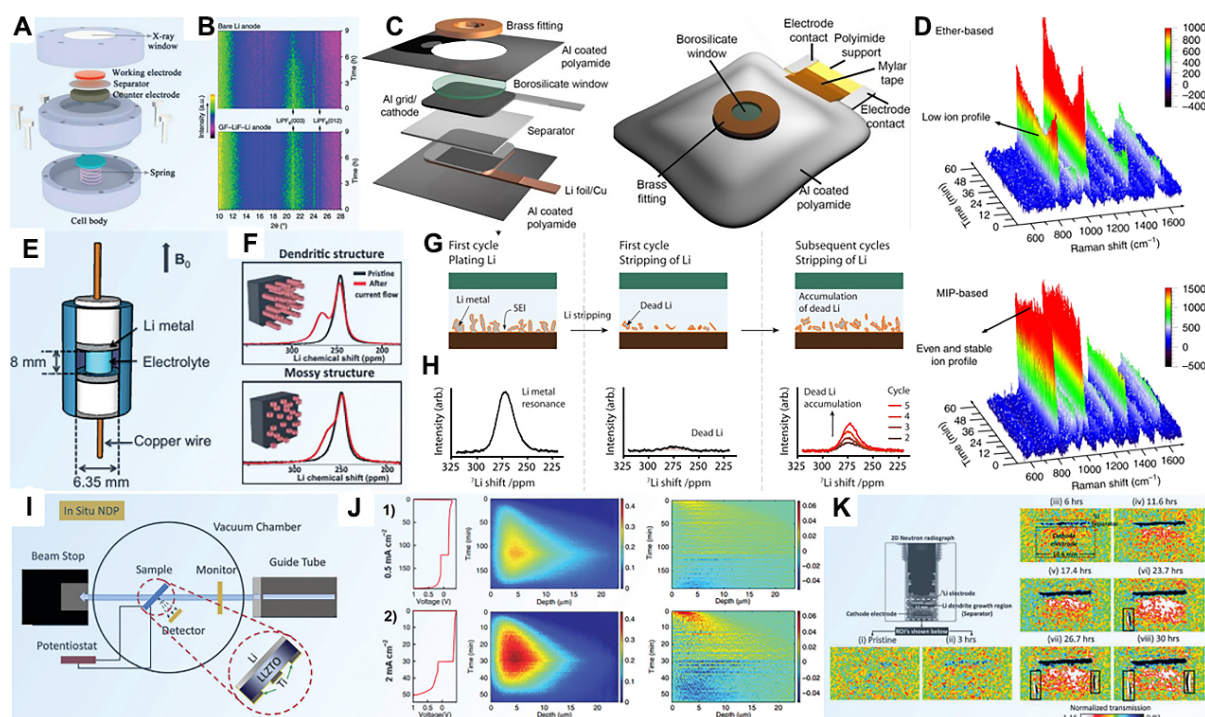


Figure 5. (A) Schematic illustration of *in situ* XRD cell. Reprinted with permission from Ref. [79]. Copyright (2019) Wiley-VCH. (B) *In situ* XRD patterns of (top) bare Li anode and (bottom) LiF-Li anode upon first charge-discharge process. Reprinted with permission from Ref. [80]. Copyright (2019) Springer Nature. (C) Schematic illustration of *in situ* Raman cell. Reprinted with permission from Ref. [81]. Copyright (2015) Wiley-VCH. (D) *In situ* Raman spectra of ether and MIP-based electrolytes, respectively. Reprinted with permission from Ref. [83]. Copyright (2019) Springer Nature. (E) Schematic diagram of cell used for *in situ* MRI. Reprinted with permission from Ref. [90]. Copyright (2015) American Chemical Society. (F) *In situ* NMR and susceptibility calculations enable to characterize the types of Li microstructures nondestructively in a functioning battery. Reprinted with permission from Ref. [94]. Copyright (2015) American Chemical Society. (G) Schematic of ^7Li *in situ* NMR technique used to study dead Li formation and (H) corresponding ^7Li NMR spectra. Reprinted with permission from Ref. [92]. Copyright (2020) American Chemical Society. (I) Experimental setup for *in situ* NDP measurements. Reprinted with permission from Ref. [96]. Copyright (2019) Elsevier. (J) Operando NDP measurements of first plating and stripping cycle including the plating and stripping activity at (top) 0.5 mA cm^{-2} and (bottom) 2 mA cm^{-2} . Reprinted with permission from Ref. [97]. Copyright (2018) Springer Nature. (K) 2D evolution of Li distribution as a function of charging time based on normalized neutron radiographs. Reprinted with permission from Ref. [77]. Copyright (2019) American Chemical Society.

detect the Li-ion concentration variation during electrochemical processes in real time. Romanenko *et al.* conducted a quantitative MRI study on solid-state ionic plastic crystal electrolyte-based batteries [95]. Li-ion transfer into the electrode matrix during the ongoing discharge of the anode results in partial liquefaction of the electrolyte at the metal interface. Displacement of the liquefaction front is accompanied by faster Li-ion transfer through grain boundaries at the electrode. The arrival of Li^+ ions then leads the electrolyte to be partially liquefied at the electrode interface, leading to an enhancement in the charge transmission.

NDP, which is based on low energy neutrons, can quantify the concentration of Li^+ ions directly. *In situ* NDP, as a nondestructive analysis tool, provides a feasible method to determine the electrochemical reaction sites and electromigration and kinetic processes of the metal anode. Li *et al.* exhibited the Li electrodeposition behavior in a $\text{Li-Li}_{6.4}\text{La}_3\text{Zr}_{1.4}\text{Ta}_{0.6}\text{O}_{12}$ (LLZTO)-Ti solid-state battery (with a 3D Ti electrode) by *in situ* NDP (Figure 5I) [96]. Lv *et al.* investigated the spatial heterogeneity of Li metal during deposition and dissolution processes with NDP [Figure 5J] [97]. They demonstrated the impact of high current density in reducing the Li distribution density for the first time. It was found that Li integration under low current density (0.5 mA cm^{-2}) and high current density (2 mA cm^{-2}) was significantly different, indicating the effect of initial electroplating current density on the SEI and subsequent cycles. Recently,

Song *et al.* used *in situ* NR and NT to study Li distribution dynamics^[77]. As shown in Figure 5K, Li consumption increased with time during the charge process. Further studies confirmed that high current densities result in a high density of Li deposits, while low current densities generate a low density of Li deposits and thick Li deposition, thereby forming significant “dead Li”. Titration gas chromatography (GC) techniques can be used to quantify the fraction of dead Li^[98]. Recently, Hsieh *et al.* estimated the amount of dead Li by combining GC with *in situ* ⁷Li NMR analytical techniques^[99]. Based on *in situ* holographic interferometry, in which a variation in the refractive index caused by a concentration variation of chemical species leads to a discrepancy in the optical path length between the reference and objective beams, Ota *et al.* proposed the ion concentration-dependent basal growth mechanism^[100]. The results showed that the concentration gradient of Li⁺ ions around the tip and arm of Li dendrites was steeper than that at the electrode/electrolyte interface, indicating that the local current density converged here^[101-103].

THEORETICAL INVESTIGATIONS

Advanced characterization often tends to concentrate on describing the phenomenon of the electrode process. The understanding of the underlying mechanism also requires theoretical analysis, such as simulations and calculations, which provides reliable assistance for experimental studies^[104,105]. Phase field simulations are practical tools to study the Li deposition rate in the 3D conductive host, which provides guidance for the future design of the pore structures of 3D hosts^[106]. In addition, the anode/electrolyte interface is an equally critical region that has been highlighted, especially in the field of solid-state batteries. Yang *et al.* reported an atomic model of Li deposition/dissolution at the anode/solid electrolyte interface based on large-scale molecular dynamics (MD) simulations, revealing that the sluggish kinetics of Li-ion diffusion at the anode/solid electrolyte interface was responsible for the formation of interfacial nanopores^[107]. These nanopores cause an increase in interfacial contact resistance, leading to degradation of the electrochemical performance of batteries. In addition, due to the fast diffusion of Li⁺ ions, coherent interfaces were less likely to generate nanopores, which highlights the importance of interfacial engineering and new directions for the modification of LMBs. Furthermore, through classical MD simulations, Karimi *et al.* investigated the properties of 1-butyl-1-methylpyrrolidinium tricyanomethanide (Pyr₁₄TCM), 1-butyl-1-methylpyrrolidinium dicyanamide (Pyr₁₄DCA) and their binary solutions with the respective Li salts^[108]. Compared with TCM⁻, the DCA⁻ showed less stability because DCA⁻ was closer to both cations (i.e., Pyr₁₄⁺ and Li⁺), which was more exposed to the consequent radical reactions. Therefore, the formed SEI on the anode surface with the LiDCA:Pyr₁₄DCA electrolyte system could probably be thicker.

Moreover, as a step toward understanding the surface reactions, thermodynamic energy factors determining the heterogeneity in the adsorption and desorption energy of ions are demonstrated by density functional theory calculations, specifically adsorption and migration energies. First, lithium tends to form dendrites different from some multivalent-ion systems, such as Mg, due to their intrinsic thermodynamic differences. According to Matsui's calculations, the bonding between Li atoms is much weaker than that between Mg, meaning that moving a Li atom from the bulk to surface needs less energy and this low free-energy difference means a greater tendency to form the low-dimension structure of whiskers and dendrites in the Li system^[109]. Combined with the first-principles calculations, high-throughput screening and machine learning methods are playing increasingly effective roles in the exploration of practical Li metal anodes. High-throughput quantum-chemical calculations starting with a huge molecule database can effectively select potential candidates based on abundant and accurate property evaluation. Compared with conventional trial-and-error methods, this well-established method can speed up the search and selection of optimal materials, greatly saving the expense and time costs.

ADVANCEMENTS IN LI METAL ANODE PROTECTION

Anode structural design

Inhomogeneous Li nucleation behavior due to uneven distribution of electrons and Li⁺ ions can trigger fatal Li dendrite growth. On this basis, various host strategies have been reported to homogenize the interface electric field, distribute the local current density and uniformize the Li⁺ flux. Furthermore, a stable host minimizes the volume variation to avoid stress fluctuations. The hosts usually fall into three categories: electron-conductive (EC) frameworks; ionic-conductive (IC) frameworks; mixed ion and electron-conductive (MIEC) frameworks.

3D current collectors (i.e., EC frameworks) with high specific surface areas (SSAs) are conducive to mitigating huge volume changes and reducing the local current density. For instance, 3D Cu current collectors with submicron pores have been reported to solve the dendrite issue directly due to the large pore volumes and high SSAs^[110]. Furthermore, the tip effect of the porous electrode induced the initial deposition of Li metal on the microchannel walls, which constrained dendrite growth. Because the initial Li nucleation sites evolve into bumps distributed on the current collector, whose edges are unable to capture Li ions under the electric field, insufficient Li ions preferentially tend to gather on the tip, which is known as the so-called “tip effect”, leading to dendritic deposition. Yan *et al.* explored the Li nucleation pattern on a variety of metal substrates and revealed a special growth phenomenon that depends on the substrates [Figure 6A]^[111]. The nucleation overpotentials of Li metal on Au, Ag, Zn and Mg substrates are almost zero, which can be explained by the definite solubility of these metals in Li metal, leading to solid solution buffer layers before the formation of Li metal. Carbon-based host materials can promote the energy density of batteries due to low density. For example, Zuo *et al.* used a graphitized carbon fiber host for Li anodes, which guarantees high areal capacity and metal plating/stripping efficiency, low voltage hysteresis and long lifespans^[112]. Jin *et al.* reported a Li restoration method via a biochar capsule to host iodine that can effectively rejuvenate electrochemically inactive Li based on an iodine redox chemistry^[113].

To effectively achieve the inhibition of dendrites, it is critical to adjust the charge transfer process and regulate the initial nucleation sites. Heteroatomic doping in a carbon matrix is one of the most effective methods to guide the initial Li nucleation process. Specifically, 20 carbonaceous-based species (pristine and heteroatom doped) were modeled with various dopants^[114]. As shown in Figure 6B, among the various single-doped carbon matrices, aO-carbon matrices exhibit the largest binding energy toward Li atoms, thus significantly decreasing the Li nucleation overpotential. In addition to heteroatom doping, a multivacancy defect-enriched carbon matrix was presented as the anode current collector [Figure 6C]^[115]. Furthermore, the modification of metallic oxides, such as ZnO, Co₃O₄, Cu₂O, TiO₂ and other polar particles, on carbon matrices is also an effective strategy to induce the migration and diffusion of Li⁺ ions to modify the nucleation and deposition of Li metal^[116]. Zhang *et al.* demonstrated a promising strategy based on a lithiophilic-lithiophobic gradient layer in which the bottom lithiophilic ZnO layer tightly anchors the whole layer onto the Li foil to facilitate a stable SEI formation and the top lithiophobic carbon nanotube sublayer can effectively suppress Li corrosion [Figure 6D]^[117].

It is notable that in a matrix host material with high electronic conductivity, Li deposition could undesirably take place outside the host, especially at high current densities. To resolve the problem, Yang *et al.* proposed a 3D garnet-type Li₇La_{2.75}Ca_{0.25}-Zr_{1.75}Nb_{0.25}O₁₂ framework as an IC Li host to achieve bottom-up deposition^[118]. The structure with a planar Cu current collector guarantees the bottom plating of Li deposits, while the dense garnet-type layer in the middle blocks potential dendritic growth, which prevents safety risks caused by short circuit. It is noted that the features of high ionic conductivity (3×10^{-4} S cm⁻¹) and single-ion conductive feature of the garnet electrode also favors uniform and stable Li deposition. The

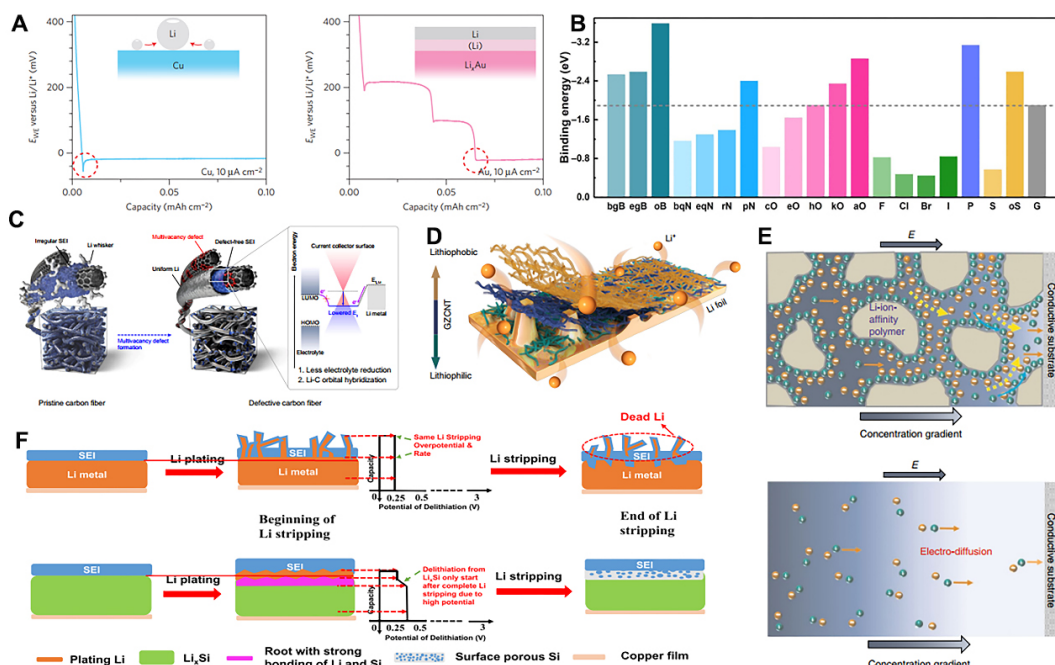


Figure 6. (A) Voltage profiles of Li deposition on Cu and Au substrates at $10 \mu\text{A cm}^{-2}$. Reprinted with permission from Ref. [111]. Copyright (2016) Springer Nature. (B) Summary of calculated binding energies between heteroatom-doped carbon and a Li atom. Reprinted with permission from Ref. [114]. Copyright (2019) American Association for the Advancement of Science. (C) Schematic of dual functionality of an electron-deficient carbon surface. Reprinted with permission from Ref. [115]. Copyright (2021) Springer Nature. (D) Schematic diagram of Li deposition on lithiophilic-lithiophobic gradient layer-coated Li foils. Reprinted with permission from Ref. [117]. Copyright (2018) Springer Nature. (E) Electrokinetic phenomena in 3D PPS under an electric field. Reprinted with permission from Ref. [124]. Copyright (2018) Springer Nature. (F) Schematic diagrams of different Li metal anode host structures. Reprinted with permission from Ref. [35]. Copyright (2019) Cell Press.

unique porous garnet structure also enlarges interfacial contact between the electrode and electrolyte, facilitating the rapid acquisition of sufficient Li^+ ions and reducing interfacial resistance significantly. Hitz *et al.* reported that Li symmetric cells based on doped $\text{Li}_7\text{La}_3\text{Zr}_2\text{O}_{12}$ ceramic Li-conductor electrodes are able to cycle at an ultrahigh current density of 10 mA cm^{-2} with an ultralow interfacial resistance of 7Ω at room temperature [119].

Apart from the reduced local current density and mitigated Li-ion depletion via optimized 3D EC and IC scaffolds, the stability of Li metal electrodes at large current densities is a complicated dynamic issue. Both electron and ion transport need to be strengthened under high rates [120]. Based on previous knowledge, different electron/ion transport rates are required for Li plating and stripping processes during high current density operation. During the Li plating process, the fast electron transport is beneficial for the efficient distribution of electrons on the electrode surface, which induces a homogenous distribution of the local current density, leading to the inhabitation of the dendrite propagation. In contrast, during the Li stripping process, the rapid transport of Li^+ ions seems to be more desirable because rapid Li^+ departure and homogenized Li^+ flux can accelerate and stabilize its dissolution according to the principle of chemical equilibrium. Therefore, the rational design of 3D MIEC frameworks is considered as a promising solution and has attracted significant attention. Considering that Li anodes with excess Li capacity are needed to offset irreversible Li loss during cycling in full batteries due to continuous parasitic reactions, it is a rational strategy for employing MIEC anodes through molten infusion technique on a large scale. Guo *et al.* reported that molten Li could be successfully absorbed into the channels of carbon wood modified with ZnO nanoparticles, forming a Li/carbon wood composite anode that enabled a homogeneous Li^+ flux

behavior^[121]. More recently, Luo and co-workers proposed a 3D MXene aerogel MIEC scaffold for a Li metal anode with excellent electrochemical performance under high current density^[122]. Represented by Ti_3C_2 , such MXene aerogels have both high electronic conductivity and fast ionic transport capability due to the abundant lithiophilic oxygen- and fluorine-containing functional groups.

In addition, some IC frameworks, such as $Li_{6.4}La_3Zr_2Al_{0.2}O_{12}$ (LLZO), were incorporated into the 3D EC framework of carbon nanofibers via an electrospinning process, followed by heat treatment, fabricating a 3D MIEC composite framework^[123]. The outstanding performance of this framework could be attributed to the improved electrolyte wettability caused by decreased interface energy and homogenized Li^+ flux to compensate Li^+ depletion in the vicinity of the electrode. Li *et al.* developed a 3D crosslinked porous polyethylenimine sponge (PPS), which was capable of providing strong Li-ion affinity and promoting electrokinetic phenomena [Figure 6E]^[124]. The lithiophilicity of the PPS concentrates Li^+ ions in the sponge, leading to a higher local concentration of Li^+ ions at the electrode/electrolyte interface compared to that in the bulk electrolyte. Chen *et al.* reported that a prelithiated Li_xSi anode can effectively suppress the formation of dead Li when the total lithiation/delithiation capacity in each cycle is higher than the Li plating/stripping capacity on Li_xSi because the slight delithiation from Li_xSi shows a higher potential than the stripping of deposited Li from Li_xSi [Figure 6F]^[125].

Fabrication of artificial interfaces

Fabricating artificial SEIs (ASEIs) is one of the most attractive solutions to overcome the shortcomings of spontaneously formed interphases. Due to multiple degrees of freedom, ASEIs with unique properties and compositions created outside an electrochemical cell can be precisely tuned. A stable and homogeneous ASEI with a specific composition on the electrode surface is favorable for the definition and characterization of structure-property relationships. Ideally, as shown in Figure 7A, an ideal ASEI must meet several intrinsic requirements: (1) chemically and electrochemically stable to avoid parasitic reactions with the electrolyte; (2) mechanically flexible and robust to withstand the volume change and retard dendrite growth during repeated cycles; and (3) uniform and abundant ion conductive pathways to facilitate facile single Li-ion diffusion^[125,126].

An ideal ASEI must be stable to the Li metal anode, preventing electrolyte component decomposition apart from the reduction of Li^+ ions^[127]. Polymer networks have shown the ability to stabilize Li metal anodes and block electrolyte penetration to some extent. In addition, ASEIs are attractive due to the polymer networks, such as polyethylene oxide^[128], Nafion^[129] and polyvinylidene fluoride^[130], having a maximum limit in swelling due to the balance between the entropy of mixing and the entropy of the polymer chain configuration^[131]. Huang *et al.* integrated tether cations onto a polymer backbone to form a polyionic liquid coating that is chemically stable even at ultranegative potentials below Li reduction (< -3.04 V vs. SHE), resulting in an improved Li deposition morphology, as well as superior cycling performance of LMBs [Figure 7B]^[132]. A Li metal electrode featured with an air-stable and waterproof surface using a PEO-based composite ASEI film was also prepared by Yang and co-workers for Li-S battery applications [Figure 7C]^[133].

The mechanical modulus of the interphase can be tuned by modulating the physical structure and chemical compositions of the ASEI. During the electrodeposition process, mechanically unstable SEIs are prone to fracture and allow dendritic penetration when confronted with large amounts of stress and strain, leading to the generation of hotspots in which uneven diffusion of Li^+ ions aggravates dendritic Li growth^[134]. Even without dendrites, the mechanical degradation of the SEI will expose fresh Li to solution, leading to the consumption of both electrolyte and Li metal. Therefore, the degradation of mechanical stabilities accelerates the failure of batteries. Tamwattana *et al.* showed that the considerably high tensile strength and

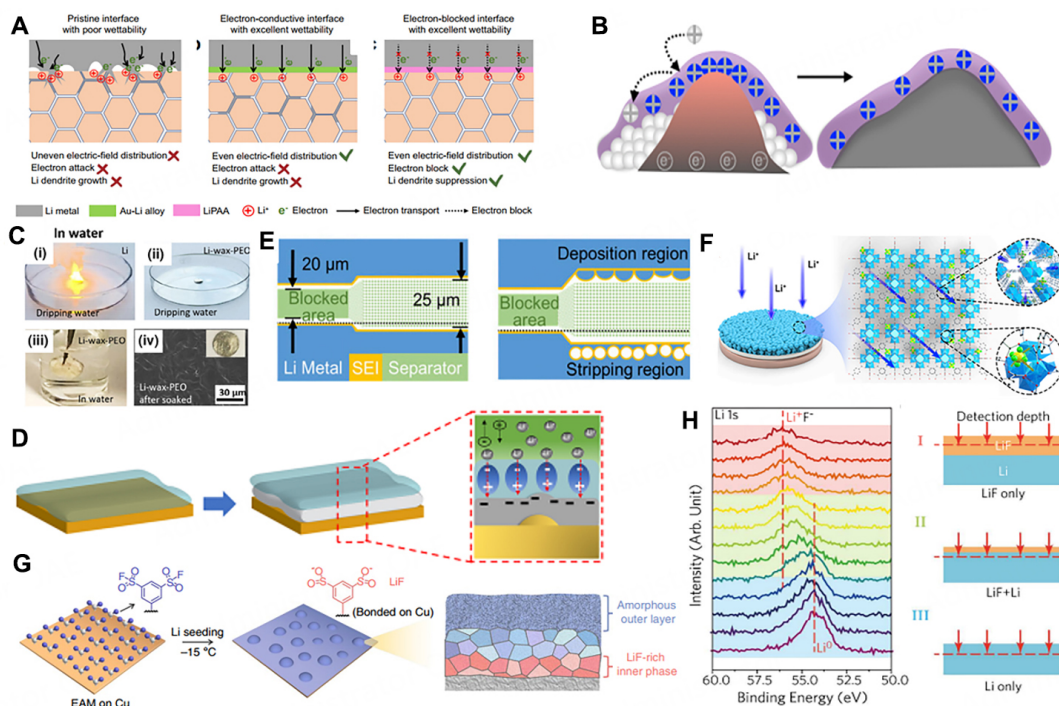


Figure 7. (A) Schematic illustrations of Li deposition at various interfaces. Reprinted with permission from Ref.^[125]. Copyright (2021) Springer Nature. (B) Polyionic liquid coating on Li metal anode. Reprinted with permission from Ref.^[132]. Copyright (2020) American Chemical Society. (C) Stability comparison of PEO-coated Li and bare Li in water. Reprinted with permission from Ref.^[133]. Copyright (2020) Elsevier. (D) Schematic illustrations of mitigated surface concentration polarization with an artificial SEI with a high dielectric constant. Reprinted with permission from Ref.^[135]. Copyright (2021) American Chemical Society. (E) Schematic of half-blocked coin cell before charging and after first charging. Reprinted with permission from Ref.^[143]. Copyright (2018) National Academy of Sciences. (F) MOF-based SSI formed on LMA with immobilized ionic channels for fast Li^+ transport. Reprinted with permission from Ref.^[148]. Copyright (2020) Cell Press. (G) Uniform and stable ASEI on Cu. Reprinted with permission from Ref.^[150]. Copyright (2020) Springer Nature. (H) XPS depth profiles of Li 1s with three stages in regions I (red), II (green) and III (blue), with the detection depth of XPS covering only the LiF layer, LiF+Li and Li, respectively. Reprinted with permission from Ref.^[151]. Copyright (2017) American Chemical Society.

Young's modulus in α -PVDF are attributable to a dense microstructure and less porosity, which can effectively promote a uniform Li deposition by decreasing the overpotential, lowering the local current density and suppressing Li protrusions [Figure 7D]^[135,136]. A flexible Young's modulus (1-0 GPa) for an ASEI can be achieved with semi-crystalline and crystalline polymers that can increase the strength of the backbone. In contrast, inorganics, such as ceramics, generally provide a high Young's modulus (10-100 GPa), which enables resistance to the stress imposed by the growing dendrites (4.2 GPa). Furthermore, Li-ion conductive inorganics, like Li_3N ^[137], LiF ^[138], Li_2S ^[139] and Li_3PO_4 ^[140], as well as passive inorganics that solely impart mechanical stiffness at the interface, like Al_2O_3 ^[141] and nano-diamond coatings^[142], are considered as high mechanical modulus candidates.

The heterogeneous transport of Li^+ ions in the native SEI is due to differences in diffusion rates in different regions, which is the main triggering factor of dendrites. Maintaining fast and uniform Li-ion flux is critical to suppressing the formation of dendrites. Shi *et al.* revealed the stripping mechanism on a Li anode by visualizing the interface between the stripped Li and the SEI [Figure 7E]^[143]. After the cations migrate through the SEI layer, the metal vacancies will be left on the Li electrode below the SEI layer. The aggregation of metal vacancies can lead to the formation of large cavities at the Li/SEI interface, which is fatal for the adherence of the SEI layer. Tewari *et al.* revealed that ion depletion easily resulted in a scarcity

of Li^+ ions beneath the SEI, thereby making it a diffusion-controlled reaction. Reaction-controlled rather than diffusion-controlled conditions are favorable for compact and stable deposition^[144]. Lithiated Nafion™ was reported as a single ion-conducting polymer to fabricate an ASEI^[145,146]. Crosslinked ionic networks offer the multifunctionality of both electrolyte blocking and single ion conduction^[147]. Xu *et al.* proposed that coating an ion-transport rectifier on the Li metal anode allows the anions (e.g., PF_6^-) to complex with the Lewis acid sites and the solvated cations (Li^+) to effectively translocate within the pore channels with both high σ_{Li^+} and t_{Li^+} [Figure 7F]^[148]. Apart from the diffusivity of ions within the interphase, the surface diffusivity also has a significant influence on the Li deposition morphology. High surface diffusivity is generally enabled by halides, such as LiF, LiBr and LiI^[149]. Gao *et al.* reported a self-assembled monolayer of electrochemically active molecules that regulates the composition and nanostructure of the SEI [Figure 7G]^[150]. A multilayer SEI that contains an amorphous outer layer and a LiF-rich inner phase seals the Li anode effectively. Lin *et al.* also developed a conformal LiF coating technique on Li surface with commercial Freon R134a as the reagent [Figure 7H]^[151].

Electrolyte modification

In general, the interaction between electrolyte solvent molecules plays a critical role in deciding the bulk properties of an electrolyte, such as the dielectric constant, boiling and melting points and viscosity, which is largely driven by van der Waals forces and tends to be much weaker than the other interactions among the solvent, cations and anions. As shown in Figure 8A, the strategies of electrolyte modification can be divided into three classes based on the regulation of the interactions in the electrolyte system: (1) regulating the interaction between the cations and solvent to modulate the redox stability of solvent molecules; (2) regulating the interaction between cations and anions to optimize the formation of solvent separated ion pairs (SSIPs), contact ion pairs (CIPs) and aggregates (AGGs) and salt solubility; and (3) regulating the interaction between the anions and solvent to adjust the anion solvation behavior^[152].

In electrolytes, especially in non-aqueous systems, Li^+ ions are generally solvated by the surrounding solvent molecules. Thus, the cation-solvent interactions have an important impact on guiding the cation solvation/desolvation and transport behavior. For example, the Li^+ solvation structure can be intuitively tuned by adjusting the electrolyte compositions. The components featuring a high Gutmann donor number are more favorable to be recruited into the inner solvation shell. Frontier molecular theory can be employed to uncover the redox stability of the modified solvation shell. The coordinated Li^+ ions attract electrons from the solvent molecules and correspondingly lower their LUMO^[153]. In the electrolyte, the solvent molecules coordinated with Li^+ ions can obtain electrons much more easily from the anode than free solvent molecules, leading to electrolyte decomposition. Therefore, according to the different affinities of solvents toward Li^+ ions, the chemical and electrochemical stabilities of electrolytes can be regulated and designed. For example, fluoroethylene carbonate (FEC) possesses a lower LUMO energy level than DEC and EC and can more easily obtain electrons from the electrode due to the strong electron-withdrawing effect of the F functional group^[154]. Consequently, FEC preferentially reacts with the Li anode to induce a LiF-rich SEI. Zhang *et al.* created a highly stable organic interphase with a well-tuned LUMO energy to improve the anti-reduction ability of SEI components and enhance the long-term cyclability of LMBS^[155,156]. Introducing trifluoromethyl functional groups ($-\text{CF}_3$) to the molecular structure in the SEI can significantly tune the orbital energies and the HOMO/LUMO gap due to the strong electron-withdrawing property of $-\text{CF}_3$ functional groups [Figure 8B]^[155,156].

In contrast to aqueous electrolytes, where anions and cations are completely separated by the solvent molecules, organic solvents tend to possess much lower dielectric constants than water and the cation-anion interaction cannot be weakened effectively. Consequently, Li salts cannot be dissociated completely, and therefore the Li^+ -anion interaction significantly affects the coordination of SSIP, CIP and AGGs, further

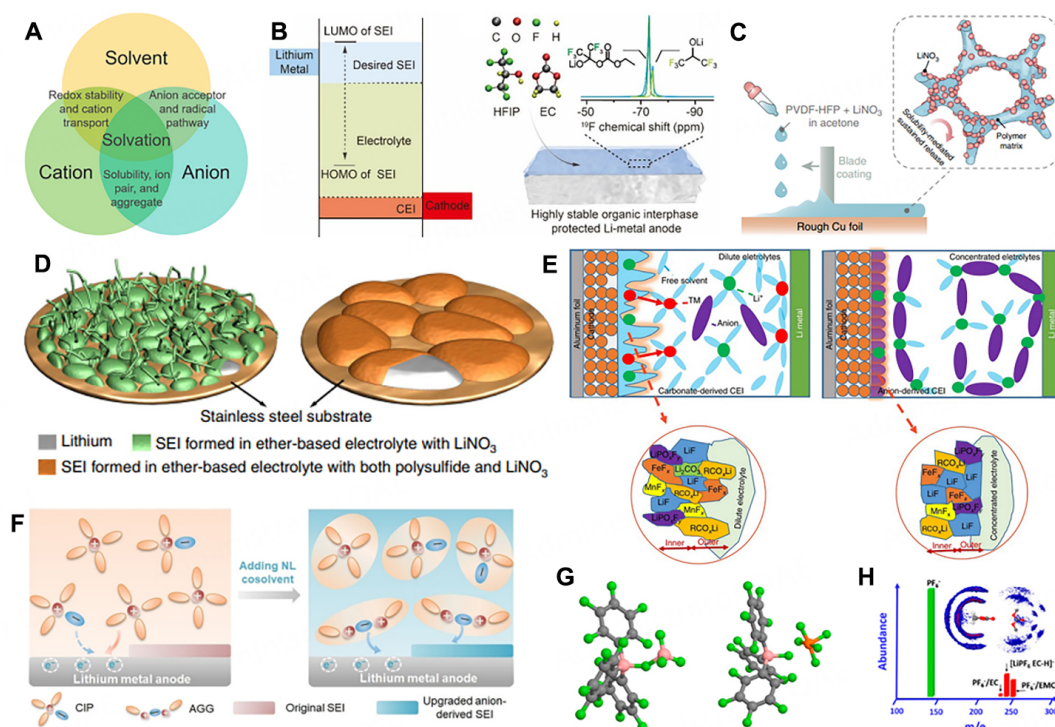


Figure 8. (A) Schematic of interaction relationship in electrolytes. Reprinted with permission from Ref.^[152]. Copyright (2020) American Chemical Society. (B) Schematic illustrations of interfacial stability enabled by the HOMO-LUMO gap of SEI and stable SEI treated chemically by fluorination. Reprinted with permission from Ref.^[156]. Copyright (2019) American Chemical Society. (C) Schematic illustration of fabrication and working principle of LNO-SRF. Reprinted with permission from Ref.^[158]. Copyright (2018) Springer Nature. (D) Schematic of morphologies of Li deposited on substrate in different electrolytes. Reprinted with permission from Ref.^[160]. Copyright (2015) Springer Nature. (E) Schematic illustrations of passivation films with 1 M and 3 M LiPF₆ in a mixed solvent of EC-EMC-DMC (1:1:1 by vol.). Reprinted with permission from Ref.^[163]. Copyright (2020) Springer Nature. (F) Schematic illustrations of effect of NL cosolvent on solvation structures and thereafter the SEI formation process. Reprinted with permission from Ref.^[164]. Copyright (2020) Wiley-VCH. (G) Optimized geometrical structures of (left) TPFPB-BF₄⁻ and (right) TPFPB-PF₆⁻ complexes. (H) Typical mass spectra via electrospray ionization and (inset) 3D isosurface rendering of F in PF₆⁻ around DMC and EC molecules. Reprinted with permission from Ref.^[165]. Copyright 2015 American Chemical Society.

regulating the features of the SEI components. In commercial dilute electrolytes, Li⁺ ions are generally solvated by the electrolyte solvent molecules with the SSIP structure, leading to a solvent-derived SEI. To avoid this structure, many anion additives, like LiNO₃, have been widely developed as effective electrolyte additives to induce CIP structures for fabricating stable anion-derived SEI and realizing uniform Li deposition^[157-159]. Liu *et al.* found that the previous knowledge regarding the preferential reduction of nitrate anions during SEI formation in ether-based electrolytes can be extended to carbonate-based systems despite their extremely limited solubility, which has a positive effect on the ion transport and charge transfer kinetics, dramatically altering the nuclei from dendritic to spherical [Figure 8C]^[158]. Li *et al.* introduced both Li₂S₈ and LiNO₃ additives to an ether-based electrolyte, which enabled a synergistic effect on the Li surface that can effectively minimize the electrolyte decomposition and prevent dendrites from propagating [Figure 8D]^[160].

More effectively, the concept of high-concentration electrolytes (HCEs) has been widely accepted^[161]. With increasing salt concentration, the number of free solvent molecules decreases, leading to an increase in the proportion of anions in the solvation shells. The involved coordination of anions transforms the Li⁺ solvation structure from SSIP to CIP and AGGs, which induces an inorganic-rich SEI and stabilizes Li metal anodes^[90,162]. Liu *et al.* found that both a favorable SEI and cathode electrolyte interphase (CEI) can be

formed in HCEs [Figure 8E]^[163]. However, an ultrahigh concentration of Li salt commonly sacrifices the ionic conductivity of electrolytes, leading to batteries with high costs. To maintain the favorable solvation structure, non-solvating fluorinated ethers with weak interactions with cations have been innovatively adopted to decorate the electrolyte, which decreases the apparent concentration of the lithium salt and retains the same solvation structure as that in the HCEs. Therefore, local HCEs that function similarly to HCEs but with reduced viscosity, improved ionic conductivity and reduced costs have been reported. Ding *et al.* reported that a type of non-solvating and low-dielectric (NL) cosolvent can intrinsically facilitate the anion-cation interaction and thus promote the proportion of AGGs via model investigations [Figure 8F]^[164].

Unlike both nucleophilic and electrophilic aqueous solvents, the electrolyte solvents employed in LMB systems are nucleophilic to prevent active protonation reactions from occurring. Furthermore, Li salts possessing anions with large ionic radii are generally adopted to guarantee ideal solubility in organic solvents with small dielectric constants. The delocalized charges and large radii of the anions both weaken the interaction between cations and solvent molecules. As a result, in most cases, the anions in electrolytes are conventionally considered to be unsolvated and the solvation of anions is rarely investigated. Nevertheless, the solvation behavior of anions inevitably influences the stability of anions and solvent molecules, the anion diffusivity and the transference number of cations. Furthermore, solvation might achieve the stability of the radicals in the electrolyte, leading to the inhibition of parasitic interfacial reactions. Solvents with a high acceptor number (AN) are expected to interact strongly with anions in the electrolyte. For instance, tris(pentafluorophenyl)borane (TPFPB) with the electron-deficient B element acting as the high AN solvent could strongly interact with PF⁶⁻ and BF⁴⁻, with free energy variations of -12.7 and -24.4 kcal mol⁻¹, respectively [Figure 8G]^[165]. These free energy variations are significantly more obvious than those between routine ester solvents and anions, which are mostly achieved by H-F interactions [Figure 8H]. In addition, cyclic carbonates rather than linear counterparts are favorable due to the greater polarity with the ring constraint. The effect of anions on the solvent molecule stability is contrary to that of cations, which improves the reductive stability and reduces the oxidative stability. In addition, the anion-solvent complexes lower the mobility of anions, thus increasing the transference number of the cations, which is conducive to the electrochemical rate performance. Furthermore, the anion solvation promotes salt dissociation and increases the solubility of the salt.

Replacing flammable liquid electrolytes with non-flammable SSEs is a feasible method to improve the safety of batteries. Current SSEs can be divided into three categories: polymer SSEs; inorganic ceramic SSEs; polymer/ceramic composite SSEs. Polymer electrolytes exhibit better flexibility and thus better interfacial contact with the Li electrode. However, their relatively low ionic conductivity and narrow electrochemical window limit their application in high-voltage batteries. Ceramic electrolytes usually possess desirably high moduli for dendrite suppression and high ionic conductivity. However, most inorganic ceramics are fragile, which restricts their application in mass production. Therefore, polymer/ceramic composite electrolytes are promising for achieving high conductivity and proper flexibility in practical LMBs. Because of the high ionic conductivity and thermal stability of PEO, it is frequently used to fabricate polymer/ceramic composite electrolytes. PEO-in-ceramic electrolytes (80% ceramic)^[166], polyvinylidene fluoride-hexafluoropropylene/Li_{1.3}Al_{0.3}Ti_{1.7}(PO₄)₃^[167,168], Li₇P₃S₁₁-PEO-LiClO₄^[169], Li_{0.33}La_{0.557}TiO₃ nanofiber-enhanced PEO^[170] and Li_{6.4}La₃Zr_{1.4}Ta_{0.6}O₁₂/PEO/succinonitrile^[171] have been successfully used as novel composite electrolytes.

Separator modification

The most direct and simple approach to protect LMBs from short circuit is blocking the growth of Li dendrites. However, conventional PP- and PE-derived separators can be easily pierced by sharp dendritic

Li^[172]. Stiff coating layers can effectively enhance the penetrating resistance of the separators. Liang *et al.* reported that curved surfaces are more favorable for dendrite suppression due to the fact that they can resist puncture from the sharp tips of Li dendrites by redistributing the interfacial stress^[173]. Based on this perspective, they proposed a separator with the coating layer of a nano-shield, like SiO₂ spheres, which can minimize the piercing force of Li dendrites and significantly improve the cycling life of LMBs. The nano-shield protection theory is applicable to polystyrene sphere-coated separators, which can extend the discharging lifespan of Li/Li symmetric cells to 70 h. Based on the same principle, Al₂O₃^[174]- and AlN^[175]-coated separators were further used to suppress dendrite growth by enhancing the mechanical barrier. In addition to inorganic coating materials, integrated separators consisting of polymers with high strength are another strategy for the suppression of dendritic growth. For example, Hao *et al.* prepared a poly(p-phenylene benzobisoxazole) PBO nanofiber membrane-based separator with high strength via a highly scalable blade casting process^[176]. These membranes possess a strength of 525 MPa, a Young's modulus of 20 GPa, a thermal stability of up to 600 °C and impressively low ionic resistance, thereby enabling the inhibition of dendrites in electrochemical cells^[176].

The irregular pores and skeletal structures of conventional separators lead to an inhomogeneous flux of Li⁺ ions due to the crowded Li⁺ ions in the pores during transport. However, the Li-ion concentration in the vicinity of the skeletons remains unchanged. Under this condition, while the Li⁺ ions reach the anode surface and obtain electrons to be reduced, the nonuniform Li deposition and formation of dendritic Li occurs. Therefore, the redistribution of Li-ion flux is crucial to inhibit the dendritic formation of LMBs. For example, ceramic and gel electrolytes with rapid Li-ion conductivity are generally employed in functional separators for balancing the Li-ion distribution^[177,178]. Compared with separators with electron-conducting coating layers, Li-ion conductor-modified separators can avoid Li reduction in the coating layer due to the fact that Li-ion conductors are electrically insulated. Furthermore, these separators possess remarkable flexibility in composition and structure for ion redistribution compared to commercial separators. Ma *et al.* proposed a 3D-ordered microporous separator using regenerated eggshell^[179]. Cations can transfer in 3D, leading to superior electrochemical performances compared to batteries with conventional separators. Similarly, Zhao *et al.* proposed that LLZTO ceramic modulated PP separators can be used as rectifiers to redistribute Li⁺ ions for dendrite-free LMBs [Figure 9A]^[180]. The separator with a LLZTO coating layer achieved the uniformity of ion concentration [Figure 9B]. Liu *et al.* decorated conventional Celgard separators with metallic Mg nanoparticles [Figure 9C]^[181]. Due to lithiophilic Mg nanoparticles, Li⁺ ions prefer to homogeneously electroplate on the separator surface, which faces the anode side. Hao *et al.* developed MOFs coated on a functionalized PP separator to regulate ion transport [Figure 9D]^[182]. The well-defined intrinsic nanochannels in MOFs and the negatively charged channels both restrict the free migration of anions, contributing to a high Li⁺ transference number of 0.68. Sheng *et al.* reported the effective suppression of electrolyte-Li metal reactivity through a nanoporous separator [Figure 9E]^[183]. Calculations assisted by diversified characterization reveal that the separator partially desolvates Li⁺ in space created by its uniform nanopores and deactivates solvents before Li deposition occurs. The surface contact gaps between the Zr-MOCN@PP and Li electrode are significantly mitigated compared to those between the UiO-66@PP separator and Li electrode [Figure 9F]. Li *et al.* reported a polyacrylamide-grafted graphene oxide molecular brush-modified PP separator [Figure 9G]^[184]. Furthermore, Liu *et al.* developed an approach to immobilize Li⁺ ions by coating the separator with functionalized nanocarbon (FNC), leading to Li dendrites growing toward each other simultaneously from both the FNC layer on the separator and the Li metal anode, which changes the Li growth direction [Figure 9H]^[185].

Generally, it is difficult to detect Li dendrites before the eventual short circuit and battery failure. However, before the battery short circuit, dendritic Li must first reach the separator, which can act as an alarm to

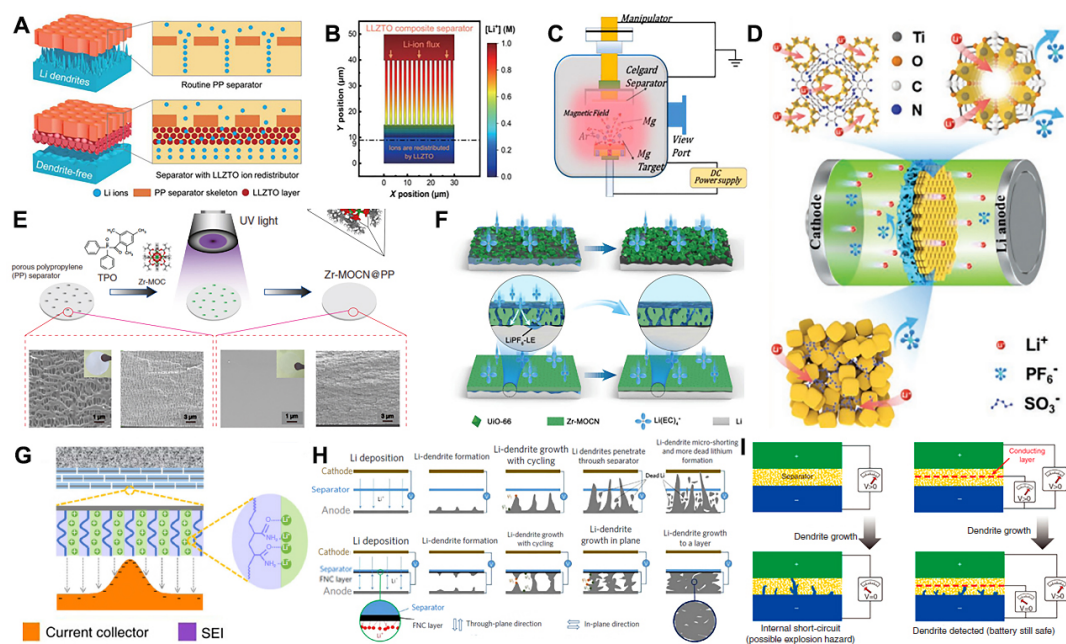


Figure 9. (A) Schematic illustration of Li deposition behavior with PP separator and LLZTO-coated separator. (B) Simulation of Li-ion distribution through LLZTO-coated separator. Reprinted with permission from Ref. [180]. Copyright (2018) American Association for the Advancement of Science. (C) Schematic illustration of magnetron sputtering system for preparation of Mg-coated separator. Reprinted with permission from Ref. [181]. Copyright (2019) Elsevier. (D) Schematic illustration of MOFs@PP separator regulating the transport of Li^+ and anions in LMBs. Reprinted with permission from Ref. [182]. Copyright (2021) Wiley-VCH. (E) Fabrication of Zr-MOCN@PP membrane via photopolymerization and corresponding SEM images. (F) Schematic illustration of Li deposition in cells with different separators: (top) UiO-66@PP; (bottom) Zr-MOCN@PP. Reprinted with permission from Ref. [183]. Copyright (2022) Springer Nature. (G) Schematic illustration of Li deposition with GO-g-PAM-modified separator. Reprinted with permission from Ref. [184]. Copyright (2017) Springer Nature. (H) A blank cell with (top) pristine separator and (bottom) FNC cell using FNC-coated separator. Reprinted with permission from Ref. [185]. Copyright (2014) Springer Nature. (I) Schematic diagrams of Li dendrite detection in (left) routine and (right) dual-layer separator-based cell. Reprinted with permission from Ref. [146]. Copyright (2017) Wiley-VCH.

detect Li dendrites. Thus, a functional separator was designed with a sensing terminal to realize dendrite detection [Figure 9I] [146]. The separator evolved into a triple-layer configuration of polymer-metal-polymer. The voltage gap between the anode and the sandwiched metal can be identified by the electrochemical potential difference. During the charge process, once Li dendrites appeared and expanded until they eventually reached the sensing metal layer, a sharp voltage drop can be effectively recorded to indicate dendritic Li growth. Once this is detected, the working battery is terminated to avoid the final short circuit, battery thermal runaway, possible fire circumstance and even potential explosion. Apart from the detection of dendrites, the sensing layer can even eliminate Li dendrites via incorporation with the Li metal reactive materials. It is reported that a nanosized Si layer sandwiched between two layers of conventional polyolefin separators can ensure the high safety of LMBs [186].

These strategies to suppress dendrite growth in LMBs, such as anode structural design, artificial SEI layers and electrolyte and separator modification, are summarized in Table 1. Each one of them seems weak for practical applications when facing tough and indomitable Li metal anodes. Mutual combination and integration will be strong to face the challenges associated with Li metal anodes. For example, structured Li metal anodes have more advantages in suppressing dendrite growth in the nucleation stage. If this strategy is matched with optimized electrolytes (or other artificial SEI layer), the composite anode can hopefully reduce the side reactions of Li metal, leading to high Coulombic efficiency with a dendrite-free Li depositing morphology. In addition, the anode matrix can be designed to tightly contact the solid-state electrolyte to reduce the interfacial impedance. Therefore, safe and high rate LMBs can be obtained.

Table 1. Summary of various protection strategies for reported Li metal anodes

No.	Strategy	Current density (mA cm ⁻²)	Nucleation potential (mV)	CE (%)	Lifespan (h)	Ref.
1	Graphitized carbon fibers	0.5	10	98.0	300	[112]
2	Iodine-carbon composite	1	/	99.9	1000	[113]
3	Electron-deficient carbon	0.1	15	98.6	170	[115]
4	ZnO/CNT	2	31	99.5	100	[117]
5	Polyionic liquid coating layer	0.5	/	99.1	500	[132]
6	LiF-rich layer	1	/	99.0	350	[138]
7	3D Al ₂ O ₃ artificial layer	1	10	95	25	[141]
8	Double-layer nanodiamond interface	1	/	99.4	150	[142]
9	Fluoroethylene carbonate additives	0.5	38	98.0	100	[154]
10	Lithium nitrate additives	1	/	99.8	300	[157]
11	Nitrate additives	1	28	98.1	200	[160]
12	Lignosulfonate additives	1	/	96.0	160	[162]
13	Al ₂ O ₃ -coated separator	0.2	/	92.3	100	[174]
14	Aluminum nitride-coated separator	0.2	11	92.0	100	[175]
15	Al-doped Li _{6.75} La ₃ Zr _{1.75} Ta _{0.25} O ₁₂ (LLZTO)-coated PP separator	1	/	98.0	450	[180]
16	Mg-coated separator	0.5	16	94.0	400	[181]

CONCLUSIONS AND OUTLOOK

In recent decades, scientists have devoted their efforts to overcoming the dilemmas of Li metal anodes. Various models (including the electromigration-limited Chazalviel, surface tension and diffusion models) are reported to explain the inner mechanism of Li plating/stripping and provide guidance for experimental operation. Various potential strategies, such as anode structural design, SEI interface modification, electrolyte optimization and separator modification, related to Li plating/stripping behavior, are proposed to stabilize Li metal anode based on the above achievements. Despite the significant breakthroughs in dealing with anodic issues, there are a number of obstacles that limit the practical application and commercialization of LMBs, which need to be addressed.

1. Non-aqueous organic electrolytes are generally adopted for LMBs, which also show inevitable instability of the interface between the electrolyte and metallic Li. The in-depth understanding of the formation mechanism, concrete constituent and specific structure of the SEI is still inadequate. It is necessary to comprehensively consider the exact role of the SEI, the precise process of Li⁺ ions crossing the SEI and the controllable modification of the SEI.

2. *In situ* characterization analyses are critical to reveal the Li plating/stripping behavior. The OM technology is only useful for microscale morphological analysis due to its low spatial resolution. Electron microscopies possess high spatial resolutions and thus research at the nanoscale is enabled by these techniques. However, electron microscopy characterizations are limited by damage to the samples caused by the electron beam and high vacuum conditions. The chemical composition of surface reaction products can be obtained by XRD, XPS, Raman and FTIR analysis. The Li quantification can be obtained by the NMR, MRI and NDP analysis. These concentration gradients of salts and Li⁺ ions can be determined by SRS microscopy, holographic interferometry and MRI analysis.

3. Host electrodes can both mitigate the volume variation of Li metal and homogenize the local current density. Some host preparation processes, such as solution casting and cooling, meet the requirements of large-scale industrial production. The pore structure is one of the focuses of future host's design, which influences both the capacity and rate performance of the battery. However, the low CE derived from the serious corrosion phenomenon caused by large SSA hinders the development of hosts. In addition, a single strategy cannot solve all the problems of the Li metal anode. Therefore, it is favorable to combine various strategies together to reduce the volume expansion, interfacial corrosion and dendrite growth of Li metal anodes simultaneously.

4. SSEs are attractive in dealing with the safety concerns of non-aqueous electrolyte-based batteries, such as poor chemical stability, leakage and flammability. Nevertheless, the low ionic conductivity, poor interfacial contact with Li metal and instability against Li metal remain great challenges for their commercial application.

5. In most reported work, the amount of Li is not controlled in the full battery, i.e., the ratio of negative and positive materials (N:P) is higher than 3:1, which is of little practical value for evaluation. Therefore, the N:P ratio is recommended as a key parameter for the practical application evaluation of the future full battery. Areal capacity is also a critical parameter, which affects the total battery energy density. The relative weight of current collector, separator, electrolyte and other components increases with decreasing areal capacity. The anodes of current LIBs possess an areal capacity of $\sim 3\text{-}4\text{ mAh cm}^{-2}$. However, the areal capacity of the cathode is often lower than 0.5 mAh cm^{-2} in the reported LMBs.

In summary, despite the great process made in the optimization of the Li metal anode, various strategies are problematic for the overall improvement of the electrochemical performance of LMBs. Furthermore, there is an obvious gap between electrochemical performances at the laboratory level and those at practical industrial conditions. Endeavors and breakthroughs in the research field of Li metal anodes are still required to drive the revival of LMBs.

DECLARATIONS

Authors' contributions

Conceptualization, data curation, writing - original draft: Yan Y

Conceptualization, data curation, writing - editing: Zeng T

Data curation: Liu S

Writing-review and editing, funding acquisition, supervision: Shu C, Zeng Y

Availability of data and materials

Not applicable.

Financial support and sponsorship

This work was financially supported by the National Natural Science Foundation of China (Grant No. 21905033, 52271201), the Science and Technology Department of Sichuan Province (Grant No. 2022YFG0100) and the Central Government Funds of Guiding Local Scientific and Technological Development for Sichuan Province (Grant No. 2022ZYD0045). The support from the State Key Laboratory of Vanadium and Titanium Resources Comprehensive Utilization (2020P4FZG02A) is also appreciated.

Conflicts of interest

All authors declared that there are no conflicts of interest.

Ethical approval and consent to participate

Not applicable.

Consent for publication

Not applicable.

Copyright

©The Author(s) 2023.

REFERENCES

1. Li J, Kong Z, Liu X, et al. Strategies to anode protection in lithium metal battery: a review. *InfoMat* 2021;3:1333-63. [DOI](#)
2. Dunn B, Kamath H, Tarascon JM. Electrical energy storage for the grid: a battery of choices. *Science* 2011;334:928-35. [DOI](#) [PubMed](#)
3. Tarascon JM, Armand M. Issues and challenges facing rechargeable lithium batteries. *Nature* 2001;414:359-67. [DOI](#) [PubMed](#)
4. Shu C, Wang J, Long J, Liu HK, Dou SX. Understanding the reaction chemistry during charging in aprotic lithium-oxygen batteries: existing problems and solutions. *Adv Mater* 2019;31:e1804587. [DOI](#) [PubMed](#)
5. Sun K, Peng Z. Intermetallic interphases in lithium metal and lithium ion batteries. *InfoMat* 2021;3:1083-109. [DOI](#)
6. Han Y, Liu B, Xiao Z, et al. Interface issues of lithium metal anode for high-energy batteries: challenges, strategies, and perspectives. *InfoMat* 2021;3:155-74. [DOI](#)
7. Whittingham MS. Lithium batteries and cathode materials. *Chem Rev* 2004;104:4271-301. [DOI](#) [PubMed](#)
8. Cheng X, Zhang R, Zhao C, Zhang Q. Toward safe lithium metal anode in rechargeable batteries: a review. *Chem Rev* 2017;117:10403-73. [DOI](#) [PubMed](#)
9. Hu Z, Wang C, Wang C, et al. Uncovering the critical impact of the solid electrolyte interphase structure on the interfacial stability. *InfoMat* 2022;4:e12249. [DOI](#)
10. Liu B, Zhang J, Xu W. Advancing lithium metal batteries. *Joule* 2018;2:833-45. [DOI](#)
11. Yang K, Chen L, Ma J, He Y, Kang F. Progress and perspective of $\text{Li}_{1+x}\text{Al}_x\text{Ti}_{2-x}(\text{PO}_4)_3$ ceramic electrolyte in lithium batteries. *InfoMat* 2021;3:1195-217. [DOI](#)
12. Peled E. The electrochemical behavior of alkali and alkaline earth metals in nonaqueous battery systems-the solid electrolyte interphase model. *J Electrochem Soc* 1979;126:2047-51. [DOI](#)
13. Peled E, Golodnitsky D, Ardel G. Advanced model for solid electrolyte interphase electrodes in liquid and polymer electrolytes. *J Electrochem Soc* 1997;144:L208-10. [DOI](#)
14. Aurbach D, Daroux ML, Faguy PW, Yeager E. Identification of surface films formed on lithium in propylene carbonate solutions. *J Electrochem Soc* 1987;134:1611-20. [DOI](#)
15. Aurbach D, Ein-ely Y, Zaban A. The surface chemistry of lithium electrodes in alkyl carbonate solutions. *J Electrochem Soc* 1994;141:L1-3. [DOI](#)
16. Aurbach D, Ein-eli Y, Markovsky B, et al. The study of electrolyte solutions based on ethylene and diethyl carbonates for rechargeable li batteries: II. Graphite electrodes. *J Electrochem Soc* 1995;142:2882-90. [DOI](#)
17. Ein-eli Y. A new perspective on the formation and structure of the solid electrolyte interface at the graphite anode of li-ion cells. *Electrochem Solid-State Lett* 1999;2:212. [DOI](#)
18. Goodenough JB, Kim Y. The lithium-ion battery: state of the art and future perspectives. *Chem Mater* 2010;22:587-603. [DOI](#)
19. Xu K. Nonaqueous liquid electrolytes for lithium-based rechargeable batteries. *Chem Rev* 2004;104:4303-417. [DOI](#) [PubMed](#)
20. Chazalviel J. Electrochemical aspects of the generation of ramified metallic electrodeposits. *Phys Rev A* 1990;42:7355-67. [DOI](#) [PubMed](#)
21. Peng H, Huang J, Cheng X, Zhang Q. Lithium-sulfur batteries: review on high-loading and high-energy lithium-sulfur batteries. *Adv Energy Mater* 2017;7:1700260. [DOI](#)
22. Zhang L, Yang T, Du C, et al. Lithium whisker growth and stress generation in an in situ atomic force microscope-environmental transmission electron microscope set-up. *Nat Nanotechnol* 2020;15:94-8. [DOI](#) [PubMed](#)
23. Rosso M, Chassaing E, Chazalviel J, Gobron T. Onset of current-driven concentration instabilities in thin cell electrodeposition with small inter-electrode distance. *Electrochim Acta* 2002;47:1267-73. [DOI](#)
24. Barton JL, Bockris, JOM. The electrolytic growth of dendrites from ionic solutions. *Proc R Soc Lond A* 1962;268:485-505. [DOI](#)
25. Yan Y, Shu C, Zheng R, et al. Long-cycling lithium-oxygen batteries enabled by tailoring Li nucleation and deposition via lithiophilic oxygen vacancy in $\text{Vo-TiO}_2/\text{Ti}_3\text{C}_2\text{Tx}$ composite anodes. *J Energy Chem* 2022;65:654-65. [DOI](#)
26. Diggle JW, Despic AR, Bockris JO. The mechanism of the dendritic electrocrystallization of zinc. *J Electrochem Soc* 1969;116:1503.

DOI

27. Yamaki J, Tobishima S, Hayashi K, Keiichi Saito, Nemoto Y, Arakawa M. A consideration of the morphology of electrochemically deposited lithium in an organic electrolyte. *J Power Sources* 1998;74:219-27. DOI
28. Witten TA, Sander LM. Diffusion-limited aggregation, a kinetic critical phenomenon. *Phys Rev Lett* 1981;47:1400. DOI
29. Mayers MZ, Kaminski JW, Miller TF. Suppression of dendrite formation via pulse charging in rechargeable lithium metal batteries. *J Phys Chem C* 2012;116:26214-21. DOI
30. Chandrasekar M, Pushpavanam M. Pulse and pulse reverse plating-conceptual, advantages and applications. *Electrochim Acta* 2008;53:3313-22. DOI
31. Brissot C, Rosso M, Chazalviel J-, Lascaud S. In situ concentration cartography in the neighborhood of dendrites growing in lithium/polymer-electrolyte/lithium cells. *J Electrochem Soc* 1999;146:4393-400. DOI
32. Brissot C, Rosso M, Chazalviel J, Lascaud S. Dendritic growth mechanisms in lithium/polymer cells. *J Power Sources* 1999;81-82:925-9. DOI
33. Rosso M, Brissot C, Teyssoit A, et al. Dendrite short-circuit and fuse effect on Li/polymer/Li cells. *Electrochim Acta* 2006;51:5334-40. DOI
34. Arakawa M, Tobishima S, Nemoto Y, Ichimura M, Yamaki J. Lithium electrode cycleability and morphology dependence on current density. *J Power Sources* 1993;43:27-35. DOI
35. Chen L, Fan X, Ji X, Chen J, Hou S, Wang C. High-energy Li metal battery with lithiated host. *Joule* 2019;3:732-44. DOI
36. Ye H, Zheng ZJ, Yao HR, et al. Guiding uniform Li plating/stripping through lithium-aluminum alloying medium for long-life Li metal batteries. *Angew Chem Int Ed* 2019;58:1094-9. DOI PubMed
37. Li X, Zheng J, Ren X, et al. Dendrite-free and performance-enhanced lithium metal batteries through optimizing solvent compositions and adding combinational additives. *Adv Energy Mater* 2018;8:1703022. DOI
38. Louli AJ, Eldesoky A, Weber R, et al. Diagnosing and correcting anode-free cell failure via electrolyte and morphological analysis. *Nat Energy* 2020;5:693-702. DOI
39. Jungjohann KL, Gannon RN, Goriparti S, et al. Cryogenic laser ablation reveals short-circuit mechanism in lithium metal batteries. *ACS Energy Lett* 2021;6:2138-44. DOI
40. Chan CK, Peng H, Liu G, et al. High-performance lithium battery anodes using silicon nanowires. *Nat Nanotechnol* 2008;3:31-5. DOI PubMed
41. Xu G, Li J, Wang C, et al. The formation/decomposition equilibrium of LiH and its Contribution on anode failure in practical lithium metal batteries. *Angew Chem Int Ed* 2021;133:7849-55. DOI PubMed
42. Lu D, Shao Y, Lozano T, et al. Failure mechanism for fast-charged lithium metal batteries with liquid electrolytes. *Adv Energy Mater* 2015;5:1400993. DOI
43. Li Z, Huang J, Yann Liaw B, Metzler V, Zhang J. A review of lithium deposition in lithium-ion and lithium metal secondary batteries. *J Power Sources* 2014;254:168-82. DOI
44. Colclasure AM, Li X, Cao L, Finegan DP, Yang C, Smith K. Significant life extension of lithium-ion batteries using compact metallic lithium reservoir with passive control. *Electrochim Acta* 2021;370:137777. DOI
45. Yu SH, Huang X, Brock JD, Abuña HD. Regulating key variables and visualizing lithium dendrite growth: an operando X-ray study. *J Am Chem Soc* 2019;141:8441-9. DOI PubMed
46. Conder J, Marino C, Novák P, Villevieille C. Do imaging techniques add real value to the development of better post-Li-ion batteries? *J Mater Chem A* 2018;6:3304-27. DOI
47. Osaka T, Momma T, Nishimura K, Tajima T. In situ observation and evaluation of electrodeposited lithium by means of optical microscopy with alternating current impedance spectroscopy. *J Electrochem Soc* 1993;140:2745-8. DOI
48. Steiger J, Kramer D, Mönig R. Mechanisms of dendritic growth investigated by in situ light microscopy during electrodeposition and dissolution of lithium. *J Power Sources* 2014;261:112-9. DOI
49. Steiger J, Kramer D, Mönig R. Microscopic observations of the formation, growth and shrinkage of lithium moss during electrodeposition and dissolution. *Electrochim Acta* 2014;136:529-36. DOI
50. Shen K, Wang Z, Bi X, et al. Magnetic field-suppressed lithium dendrite growth for stable lithium-metal batteries. *Adv Energy Mater* 2019;9:1900260. DOI
51. Rulev AA, Sergeev AV, Yashina LV, Jacob T, Itkis DM. Electromigration in lithium whisker formation plays insignificant role during electroplating. *ChemElectroChem* 2019;6:1324-8. DOI
52. Sagane F, Ikeda K, Okita K, Sano H, Sakaebe H, Iriyama Y. Effects of current densities on the lithium plating morphology at a lithium phosphorus oxynitride glass electrolyte/copper thin film interface. *J Power Sources* 2013;233:34-42. DOI
53. Foroozan T, Sharifi-asl S, Shahbazian-yassar R. Mechanistic understanding of Li dendrites growth by in-situ/operando imaging techniques. *J Power Sources* 2020;461:228135. DOI
54. Krauskopf T, Dippel R, Hartmann H, et al. Lithium-metal growth kinetics on LLZO garnet-type solid electrolytes. *Joule* 2019;3:2030-49. DOI
55. Motoyama M, Ejiri M, Iriyama Y. Modeling the nucleation and growth of Li at metal current collector/LiPON interfaces. *J Electrochem Soc* 2015;162:A7067-71. DOI
56. Rong G, Zhang X, Zhao W, et al. Liquid-phase electrochemical scanning electron microscopy for in situ investigation of lithium dendrite growth and dissolution. *Adv Mater* 2017;29:1606187. DOI PubMed

57. Wang P, Qu W, Song W, Chen H, Chen R, Fang D. Electro-chemo-mechanical issues at the interfaces in solid-state lithium metal batteries. *Adv Funct Mater* 2019;29:1900950. DOI
58. Huang JY, Zhong L, Wang CM, et al. In situ observation of the electrochemical lithiation of a single SnO₂ nanowire electrode. *Science* 2010;330:1515-20. DOI PubMed
59. Kushima A, So KP, Su C, et al. Liquid cell transmission electron microscopy observation of lithium metal growth and dissolution: Root growth, dead lithium and lithium flotsams. *Nano Energy* 2017;32:271-9. DOI
60. Mehdi BL, Qian J, Nasybulin E, et al. Observation and quantification of nanoscale processes in lithium batteries by operando electrochemical (S)TEM. *Nano Lett* 2015;15:2168-73. DOI PubMed
61. Gong C, Pu SD, Gao X, et al. Revealing the role of fluoride-rich battery electrode interphases by operando transmission electron microscopy. *Adv Energy Mater* 2021;11:2003118. DOI
62. Li Y, Li Y, Pei A, et al. Atomic structure of sensitive battery materials and interfaces revealed by cryo-electron microscopy. *Science* 2017;358:506-10. DOI PubMed
63. Wang X, Pawar G, Li Y, et al. Glassy Li metal anode for high-performance rechargeable Li batteries. *Nat Mater* 2020;19:1339-45. DOI PubMed
64. Aurbach D, Cohen Y. Morphological studies of Li deposition processes in LiAsF₆/PC solutions by in situ atomic force microscopy. *J Electrochem Soc* 1997;144:3355-60. DOI
65. Kitta M, Sano H. Real-time observation of Li deposition on a Li electrode with operand atomic force microscopy and surface mechanical imaging. *Langmuir* 2017;33:1861-6. DOI PubMed
66. Yoon I, Jurng S, Abraham DP, Lucht BL, Guduru PR. In situ measurement of the plane-strain modulus of the solid electrolyte interphase on lithium-metal anodes in ionic liquid electrolytes. *Nano Lett* 2018;18:5752-9. DOI PubMed
67. Krueger B, Balboa L, Dohmann JF, Winter M, Bieker P, Wittstock G. Solid electrolyte interphase evolution on lithium metal electrodes followed by scanning electrochemical microscopy under realistic battery cycling current densities. *ChemElectroChem* 2020;7:3590-6. DOI
68. Nishikawa K, Mori T, Nishida T, Fukunaka Y, Rosso M, Homma T. In situ observation of dendrite growth of electrodeposited Li metal. *J Electrochem Soc* 2010;157:A1212. DOI
69. Cheng J, Assegie AA, Huang C, et al. Visualization of lithium plating and stripping via in operando transmission X-ray microscopy. *J Phys Chem C* 2017;121:7761-6. DOI
70. Ebner M, Marone F, Stampanoni M, Wood V. Visualization and quantification of electrochemical and mechanical degradation in Li ion batteries. *Science* 2013;342:716-20. DOI
71. Harry KJ, Hallinan DT, Parkinson DY, MacDowell AA, Balsara NP. Detection of subsurface structures underneath dendrites formed on cycled lithium metal electrodes. *Nat Mater* 2014;13:69-73. DOI PubMed
72. Lewis JA, Cortes FJQ, Liu Y, et al. Linking void and interphase evolution to electrochemistry in solid-state batteries using operando X-ray tomography. *Nat Mater* 2021;20:503-10. DOI PubMed
73. Jung H, Lee B, Lengyel M, et al. Nanoscale in situ detection of nucleation and growth of Li electrodeposition at various current densities. *J Mater Chem A* 2018;6:4629-35. DOI
74. Ilott AJ, Mohammadi M, Chang HJ, Grey CP, Jerschow A. Real-time 3D imaging of microstructure growth in battery cells using indirect MRI. *Proc Natl Acad Sci USA* 2016;113:10779-84. DOI PubMed PMC
75. Sathiyaraj M, Leriche JB, Salager E, Gourier D, Tarascon JM, Vezin H. Electron paramagnetic resonance imaging for real-time monitoring of Li-ion batteries. *Nat Commun* 2015;6:6276. DOI PubMed PMC
76. Wandt J, Marino C, Gasteiger HA, Jakes P, Eichel R, Granwehr J. Operando electron paramagnetic resonance spectroscopy - formation of mossy lithium on lithium anodes during charge-discharge cycling. *Energy Environ Sci* 2015;8:1358-67. DOI
77. Song B, Dhiman I, Carothers JC, et al. Dynamic lithium distribution upon dendrite growth and shorting revealed by operando neutron imaging. *ACS Energy Lett* 2019;4:2402-8. DOI
78. Sun F, Zhou D, He X, et al. Morphological reversibility of modified Li-based anodes for next-generation batteries. *ACS Energy Lett* 2019;4:306-16. DOI
79. Xia M, Liu T, Peng N, et al. Lab-scale in situ X-Ray diffraction technique for different battery systems: designs, applications, and perspectives. *Small Methods* 2019;3:1900119. DOI
80. Shen X, Li Y, Qian T, et al. Lithium anode stable in air for low-cost fabrication of a dendrite-free lithium battery. *Nat Commun* 2019;10:900. DOI PubMed PMC
81. Ghanty C, Markovsky B, Erickson EM, et al. Li⁺-ion extraction/insertion of Ni-rich Li_{1-x}(Ni_yCo_zMn₂)_wO₂ (0.005 < x < 0.03; y:z = 8:1, w ≈ 1) electrodes: in situ XRD and raman spectroscopy study. *ChemElectroChem* 2015;2:1479-86. DOI
82. Qiu F, Zhang X, Qiao Y, et al. An ultra-stable and enhanced reversibility lithium metal anode with a sufficient O₂ design for Li-O₂ battery. *Energy Storage Mater* 2018;12:176-82. DOI
83. Chen W, Hu Y, Lv W, et al. Lithiophilic montmorillonite serves as lithium ion reservoir to facilitate uniform lithium deposition. *Nat Commun* 2019;10:4973. DOI PubMed PMC
84. Cheng Q, Wei L, Liu Z, et al. Operando and three-dimensional visualization of anion depletion and lithium growth by stimulated Raman scattering microscopy. *Nat Commun* 2018;9:2942. DOI PubMed PMC
85. Hu Z, Xian F, Guo Z, et al. Nonflammable nitrile deep eutectic electrolyte enables high-voltage lithium metal batteries. *Chem Mater* 2020;32:3405-13. DOI

86. Thirumalraj B, Hagos TT, Huang CJ, et al. Nucleation and growth mechanism of lithium metal electroplating. *J Am Chem Soc* 2019;141:18612-23. DOI PubMed
87. Schwöbel A, Hausbrand R, Jaegermann W. Interface reactions between LiPON and lithium studied by in-situ X-ray photoemission. *Solid State Ionics* 2015;273:51-4. DOI
88. Etxebarria A, Yun DJ, Blum M, et al. Revealing in situ Li metal anode surface evolution upon exposure to CO₂ using ambient pressure X-ray photoelectron spectroscopy. *ACS Appl Mater Interfaces* 2020;12:26607-13. DOI PubMed
89. Yan C, Cheng XB, Tian Y, et al. Dual-layered film protected lithium metal anode to enable dendrite-free lithium deposition. *Adv Mater* 2018;30:e1707629. DOI PubMed
90. Chang HJ, Ilott AJ, Trease NM, Mohammadi M, Jerschow A, Grey CP. Correlating microstructural lithium metal growth with electrolyte salt depletion in lithium batteries using ⁷Li MRI. *J Am Chem Soc* 2015;137:15209-16. DOI PubMed
91. Bayley PM, Trease NM, Grey CP. Insights into electrochemical sodium metal deposition as probed with in situ ²³Na NMR. *J Am Chem Soc* 2016;138:1955-61. DOI PubMed
92. Gunnarsdóttir AB, Amanchukwu CV, Menkin S, Grey CP. Noninvasive in situ NMR study of “dead lithium” formation and lithium corrosion in full-cell lithium metal batteries. *J Am Chem Soc* 2020;142:20814-27. DOI PubMed PMC
93. Chandrashekar S, Trease NM, Chang HJ, Du L-S, Grey CP, Jerschow A. ⁷Li MRI of Li batteries reveals location of microstructural lithium. *Nat Mater* 2012;11:311-5. DOI PubMed
94. Chang HJ, Trease NM, Ilott AJ, et al. Investigating Li microstructure formation on Li anodes for lithium batteries by in situ ⁶Li/⁷Li NMR and SEM. *J Phys Chem C* 2015;119:16443-51. DOI
95. Romanenko K, Jin L, Howlett P, Forsyth M. In situ MRI of operating solid-state lithium metal cells based on ionic plastic crystal electrolytes. *Chem Mater* 2016;28:2844-51. DOI
96. Li Q, Yi T, Wang X, et al. In-situ visualization of lithium plating in all-solid-state lithium-metal battery. *Nano Energy* 2019;63:103895. DOI
97. Lv S, Verhallen T, Vasileiadis A, et al. Operando monitoring the lithium spatial distribution of lithium metal anodes. *Nat Commun* 2018;9:2152. DOI
98. Fang C, Li J, Zhang M, et al. Quantifying inactive lithium in lithium metal batteries. *Nature* 2019;572:511-5. DOI
99. Hsieh Y, Leibing M, Nowak S, Hwang B, Winter M, Brunklaus G. Quantification of dead lithium via in situ nuclear magnetic resonance spectroscopy. *Cell Rep Phys Sci* 2020;1:100139. DOI
100. Ota M, Izuo S, Nishikawa K, et al. Measurement of concentration boundary layer thickness development during lithium electrodeposition onto a lithium metal cathode in propylene carbonate. *J Electroanal Chem* 2003;559:175. DOI
101. Bommier C, Chang W, Lu Y, et al. In operando acoustic detection of lithium metal plating in commercial LiCoO₂/graphite pouch cells. *Cell Rep Phys Sci* 2020;1:100035. DOI
102. Krause LJ, Jensen LD, Dahn JR. Measurement of parasitic reactions in Li ion cells by electrochemical calorimetry. *J Electrochem Soc* 2012;159:A937-43. DOI
103. Downie LE, Krause LJ, Burns JC, Jensen LD, Chevrier VL, Dahn JR. In situ detection of lithium plating on graphite electrodes by electrochemical calorimetry. *J Electrochem Soc* 2013;160:A588-94. DOI
104. Sun Y, Yang T, Ji H, et al. Boosting the optimization of lithium metal batteries by molecular dynamics simulations: a perspective. *Adv Energy Mater* 2020;10:2002373. DOI
105. Liu X, Zhang X, Chen X, et al. A generalizable, data-driven online approach to forecast capacity degradation trajectory of lithium batteries. *J Energy Chem* 2022;68:548-55. DOI
106. Zhang R, Shen X, Cheng X, Zhang Q. The dendrite growth in 3D structured lithium metal anodes: electron or ion transfer limitation? *Energy Storage Mater* 2019;23:556. DOI
107. Yang M, Liu Y, Nolan AM, Mo Y. Interfacial atomistic mechanisms of lithium metal stripping and plating in solid-state batteries. *Adv Mater* 2021;33:e2008081. DOI PubMed
108. Karimi N, Zarrabeitia M, Mariani A, Gatti D, Varzi A, Passerini S. Nonfluorinated ionic liquid electrolytes for lithium metal batteries: ionic conduction, electrochemistry, and interphase formation. *Adv Energy Mater* 2021;11:2003521. DOI
109. Ling C, Banerjee D, Matsui M. Study of the electrochemical deposition of Mg in the atomic level: why it prefers the non-dendritic morphology. *Electrochim Acta* 2012;76:270-4. DOI
110. Wang SH, Yin YX, Zuo TT, et al. Stable Li metal anodes via regulating lithium plating/stripping in vertically aligned microchannels. *Adv Mater* 2017;29:1703729. DOI PubMed
111. Yan K, Lu Z, Lee H, et al. Selective deposition and stable encapsulation of lithium through heterogeneous seeded growth. *Nat Energy* 2016;1. DOI
112. Zuo TT, Wu XW, Yang CP, et al. Graphitized carbon fibers as multifunctional 3D current collectors for high areal capacity Li anodes. *Adv Mater* 2017;29:1700389. DOI PubMed
113. Jin C, Liu T, Sheng O, et al. Rejuvenating dead lithium supply in lithium metal anodes by iodine redox. *Nat Energy* 2021;6:378-87. DOI
114. Chen X, Chen XR, Hou TZ, et al. Lithiophilicity chemistry of heteroatom-doped carbon to guide uniform lithium nucleation in lithium metal anodes. *Sci Adv* 2019;5:eaau7728. DOI PubMed PMC
115. Kwon H, Lee JH, Roh Y, et al. An electron-deficient carbon current collector for anode-free Li-metal batteries. *Nat Commun* 2021;12:5537. DOI PubMed PMC

116. Wang Q, Liu B, Shen Y, et al. Confronting the challenges in lithium anodes for lithium metal batteries. *Adv Sci* 2021;8:e2101111. DOI PubMed PMC
117. Zhang H, Liao X, Guan Y, et al. Lithiophilic-lithiophobic gradient interfacial layer for a highly stable lithium metal anode. *Nat Commun* 2018;9:3729. DOI PubMed PMC
118. Yang C, Zhang L, Liu B, et al. Continuous plating/stripping behavior of solid-state lithium metal anode in a 3D ion-conductive framework. *Proc Natl Acad Sci USA* 2018;115:3770-5. DOI PubMed PMC
119. Hitz GT, Mcowen DW, Zhang L, et al. High-rate lithium cycling in a scalable trilayer Li-garnet-electrolyte architecture. *Mater Today* 2019;22:50-7. DOI
120. Zhang Y, Luo W, Wang C, et al. High-capacity, low-tortuosity, and channel-guided lithium metal anode. *Proc Natl Acad Sci USA* 2017;114:3584-9. DOI
121. Guo W, Liu S, Guan X, Zhang X, Liu X, Luo J. Mixed ion and electron-conducting scaffolds for high-rate lithium metal anodes. *Adv Energy Mater* 2019;9:1900193. DOI
122. Zhang X, Lv R, Wang A, Guo W, Liu X, Luo J. MXene aerogel scaffolds for high-rate lithium metal anodes. *Angew Chem Int Ed* 2018;130:15248-53. DOI PubMed
123. Zhang C, Liu S, Li G, Zhang C, Liu X, Luo J. Incorporating ionic paths into 3D conducting scaffolds for high volumetric and areal capacity, high rate lithium-metal anodes. *Adv Mater* 2018:e1801328. DOI PubMed
124. Li G, Liu Z, Huang Q, et al. Stable metal battery anodes enabled by polyethylenimine sponge hosts by way of electrokinetic effects. *Nat Energy* 2018;3:1076-83. DOI
125. Huo H, Gao J, Zhao N, et al. A flexible electron-blocking interfacial shield for dendrite-free solid lithium metal batteries. *Nat Commun* 2021;12:176. DOI PubMed PMC
126. Zhao Q, Stalin S, Archer LA. Stabilizing metal battery anodes through the design of solid electrolyte interphases. *Joule* 2021;5:1119-42. DOI
127. Chai J, Chen B, Xian F, et al. Dendrite-free lithium deposition via flexible-rigid coupling composite network for $\text{LiNi}_{0.5}\text{Mn}_{1.5}\text{O}_4/\text{Li}$ metal batteries. *Small* 2018;14:1802244. DOI
128. Khurana R, Schaefer JL, Archer LA, Coates GW. Suppression of lithium dendrite growth using cross-linked polyethylene/poly(ethylene oxide) electrolytes: a new approach for practical lithium-metal polymer batteries. *J Am Chem Soc* 2014;136:7395-402. DOI PubMed
129. Cao X, Ren X, Zou L, et al. Monolithic solid-electrolyte interphases formed in fluorinated orthoformate-based electrolytes minimize Li depletion and pulverization. *Nat Energy* 2019;4:796-805. DOI
130. Dey A. Lithium anode film and organic and inorganic electrolyte batteries. *Thin Solid Films* 1977;43:131-71. DOI
131. Goodenough JB, Park KS. The Li-ion rechargeable battery: a perspective. *J Am Chem Soc* 2013;135:1167-76. DOI PubMed
132. Huang Z, Choudhury S, Gong H, Cui Y, Bao Z. A cation-tethered flowable polymeric interface for enabling stable deposition of metallic lithium. *J Am Chem Soc* 2020;142:21393-403. DOI PubMed
133. Gao S, Sun F, Liu N, Yang H, Cao P. Ionic conductive polymers as artificial solid electrolyte interphase films in Li metal batteries - a review. *Mater Today* 2020;40:140-59. DOI
134. Hao F, Verma A, Mukherjee PP. Mechanistic insight into dendrite-SEI interactions for lithium metal electrodes. *J Mater Chem A* 2018;6:19664-71. DOI
135. Tamwattana O, Park H, Kim J, et al. High-dielectric polymer coating for uniform lithium deposition in anode-free lithium batteries. *ACS Energy Lett* 2021;6:4416-25. DOI
136. Monroe C, Newman J. The impact of elastic deformation on deposition kinetics at lithium/polymer interfaces. *J Electrochem Soc* 2005;152:A396. DOI
137. Chen K, Pathak R, Gurung A, et al. Flower-shaped lithium nitride as a protective layer via facile plasma activation for stable lithium metal anodes. *Energy Storage Mater* 2019;18:389-96. DOI
138. Yuan Y, Wu F, Chen G, Bai Y, Wu C. Porous LiF layer fabricated by a facile chemical method toward dendrite-free lithium metal anode. *J Energy Chem* 2019;37:197-203. DOI
139. Chen H, Pei A, Lin D, et al. Uniform high ionic conducting lithium sulfide protection layer for stable lithium metal anode. *Adv Energy Mater* 2019;9:1900858. DOI
140. Li NW, Yin YX, Yang CP, Guo YG. An artificial solid electrolyte interphase layer for stable lithium metal anodes. *Adv Mater* 2016;28:1853-8. DOI PubMed
141. Tian R, Feng X, Duan H, et al. Low-weight 3D Al_2O_3 network as an artificial layer to stabilize lithium deposition. *ChemSusChem* 2018;11:3243-52. DOI
142. Liu Y, Tzeng Y, Lin D, et al. An ultrastrong double-layer nanodiamond interface for stable lithium metal anodes. *Joule* 2018;2:1595-609. DOI
143. Shi F, Pei A, Boyle DT, et al. Lithium metal stripping beneath the solid electrolyte interphase. *Proc Natl Acad Sci USA* 2018;115:8529-34. DOI
144. Tewari D, Mukherjee PP. Mechanistic understanding of electrochemical plating and stripping of metal electrodes. *J Mater Chem A* 2019;7:4668-88. DOI
145. Song J, Lee H, Choo MJ, Park JK, Kim HT. Ionomer-liquid electrolyte hybrid ionic conductor for high cycling stability of lithium metal electrodes. *Sci Rep* 2015;5:14458. DOI PubMed PMC

146. Tu Z, Choudhury S, Zachman MJ, et al. Designing artificial solid-electrolyte interphases for single-ion and high-efficiency transport in batteries. *Joule* 2017;1:394-406. DOI
147. Yu Z, Mackanic DG, Michaels W, et al. A dynamic, electrolyte-blocking, and single-ion-conductive network for stable lithium-metal anodes. *Joule* 2019;3:2761-76. DOI
148. Xu Y, Gao L, Shen L, et al. Ion-transport-rectifying layer enables Li-metal batteries with high energy density. *Matter* 2020;3:1685-700. DOI
149. Kim MS, Deepika, Lee SH, et al. Enabling reversible redox reactions in electrochemical cells using protected LiAl intermetallics as lithium metal anodes. *Sci Adv* 2019;5:eaax5587. DOI PubMed PMC
150. Gao Y, Rojas T, Wang K, et al. Low-temperature and high-rate-charging lithium metal batteries enabled by an electrochemically active monolayer-regulated interface. *Nat Energy* 2020;5:534-42. DOI
151. Lin D, Liu Y, Chen W, et al. Conformal lithium fluoride protection layer on three-dimensional lithium by nonhazardous gaseous reagent freon. *Nano Lett* 2017;17:3731-7. DOI PubMed
152. Chen X, Zhang Q. Atomic insights into the fundamental interactions in lithium battery electrolytes. *ACC Chem Res* 2020;53:1992-2002. DOI PubMed
153. Chen X, Shen X, Li B, et al. Ion-solvent complexes promote gas evolution from electrolytes on a sodium metal anode. *Angew Chem Int Ed* 2018;57:734-7. DOI PubMed
154. Zhang X, Cheng X, Chen X, Yan C, Zhang Q. Fluoroethylene carbonate additives to render uniform Li deposits in lithium metal batteries. *Adv Funct Mater* 2017;27:1605989. DOI
155. Shim Y. Computer simulation study of the solvation of lithium ions in ternary mixed carbonate electrolytes: free energetics, dynamics, and ion transport. *Phys Chem Chem Phys* 2018;20:28649-57. DOI PubMed
156. Zhang W, Zhang S, Fan L, et al. Tuning the LUMO energy of an organic interphase to stabilize lithium metal batteries. *ACS Energy Lett* 2019;4:644-50. DOI
157. Yan C, Yao Y, Chen X, et al. Lithium nitrate solvation chemistry in carbonate electrolyte sustains high-voltage lithium metal batteries. *Angew Chem Int Ed* 2018;57:14055-9. DOI PubMed
158. Liu Y, Lin D, Li Y, et al. Solubility-mediated sustained release enabling nitrate additive in carbonate electrolytes for stable lithium metal anode. *Nat Commun* 2018;9:3656. DOI PubMed PMC
159. Shi Q, Zhong Y, Wu M, Wang H, Wang H. High-capacity rechargeable batteries based on deeply cyclable lithium metal anodes. *Proc Natl Acad Sci USA* 2018;115:5676-80. DOI PubMed PMC
160. Li W, Yao H, Yan K, et al. Solubility-mediated sustained release enabling nitrate additive in carbonate electrolytes for stable lithium metal anode. *Nat Commun* 2015;6:1-8. DOI
161. Suo L, Borodin O, Gao T, et al. "Water-in-salt" electrolyte enables high-voltage aqueous lithium-ion chemistries. *Science* 2015;350:938-43. DOI
162. Xu R, Yan C, Xiao Y, Zhao M, Yuan H, Huang J. In situ regulated solid electrolyte interphase via reactive separators for highly efficient lithium metal batteries. *Energy Storage Mater* 2020;28:401-6. DOI
163. Liu W, Li J, Li W, Xu H, Zhang C, Qiu X. Inhibition of transition metals dissolution in cobalt-free cathode with ultrathin robust interphase in concentrated electrolyte. *Nat Commun* 2020;11:3629. DOI PubMed PMC
164. Ding JF, Xu R, Yao N, et al. Non-solvating and low-dielectricity cosolvent for anion-derived solid electrolyte interphases in lithium metal batteries. *Angew Chem Int Ed* 2021;60:11442-7. DOI PubMed
165. von Wald Cresce A, Gobet M, Borodin O, et al. Anion solvation in carbonate-based electrolytes. *J Phys Chem C* 2015;119:27255-64. DOI
166. Chen L, Li Y, Li S, Fan L, Nan C, Goodenough JB. PEO/garnet composite electrolytes for solid-state lithium batteries: From "ceramic-in-polymer" to "polymer-in-ceramic". *Nano Energy* 2018;46:176-84. DOI
167. Freitag A, Langklotz U, Rost A, Stamm M, Ionov L. Ionically conductive polymer/ceramic separator for lithium-sulfur batteries. *Energy Storage Mater* 2017;9:105-11. DOI
168. Yang L, Wang Z, Feng Y, et al. Flexible composite solid electrolyte facilitating highly stable "soft contacting" Li-electrolyte interface for solid state lithium-ion batteries. *Adv Energy Mater* 2017;7:1701437. DOI
169. Xu X, Hou G, Nie X, et al. Li₃P₂S₁₁/poly(ethylene oxide) hybrid solid electrolytes with excellent interfacial compatibility for all-solid-state batteries. *J Power Sources* 2018;400:212-7. DOI
170. Zhu P, Yan C, Dirican M, et al. Li_{0.33}La_{0.557}TiO₃ ceramic nanofiber-enhanced polyethylene oxide-based composite polymer electrolytes for all-solid-state lithium batteries. *J Mater Chem A* 2018;6:4279-85. DOI
171. Zha W, Chen F, Yang D, Shen Q, Zhang L. High-performance Li_{6.4}La₃Zr_{1.4}Ta_{0.6}O₁₂/Poly(ethylene oxide)/Succinonitrile composite electrolyte for solid-state lithium batteries. *J Power Sources* 2018;397:87-94. DOI
172. Wu H, Zhuo D, Kong D, Cui Y. Improving battery safety by early detection of internal shorting with a bifunctional separator. *Nat Commun* 2014;5:5193. DOI PubMed
173. Liang J, Chen Q, Liao X, et al. A nano-shield design for separators to resist dendrite formation in lithium-metal batteries. *Angew Chem Int Ed* 2020;132:6623-8. DOI PubMed
174. Wang Q, Yang J, Wang Z, Shi L, Zhao Y, Yuan S. Dual-scale Al₂O₃ particles coating for high-performance separator and lithium metal anode. *Energy Technol* 2020;8:1901429. DOI
175. Kim PJH, Pol VG. Surface functionalization of a conventional polypropylene separator with an aluminum nitride layer toward

- ultrastable and high-rate lithium metal anodes. *ACS Appl Mater Interfaces* 2019;11:3917-24. [DOI](#) [PubMed](#)
176. Hao X, Zhu J, Jiang X, et al. Ultrastrong polyoxazole nanofiber membranes for dendrite-proof and heat-resistant battery separators. *Nano Lett* 2016;16:2981-7. [DOI](#) [PubMed](#)
 177. Wang Y, Shi L, Zhou H, et al. Polyethylene separators modified by ultrathin hybrid films enhancing lithium ion transport performance and Li-metal anode stability. *Electrochim Acta* 2018;259:386-94. [DOI](#)
 178. Han X, Gong Y, Fu KK, et al. Negating interfacial impedance in garnet-based solid-state Li metal batteries. *Nat Mater* 2017;16:572-9. [DOI](#) [PubMed](#)
 179. Ma L, Chen R, Hu Y, et al. Nanoporous and lyophilic battery separator from regenerated eggshell membrane with effective suppression of dendritic lithium growth. *Energy Storage Mater* 2018;14:258-66. [DOI](#)
 180. Zhao CZ, Chen PY, Zhang R, et al. An ion redistributor for dendrite-free lithium metal anodes. *Sci Adv* 2018;4:3446. [DOI](#)
 181. Liu Y, Xiong S, Wang J, et al. Dendrite-free lithium metal anode enabled by separator engineering via uniform loading of lithiophilic nucleation sites. *Energy Storage Mater* 2019;19:24-30. [DOI](#)
 182. Hao Z, Wu Y, Zhao Q, et al. Advanced metal-organic framework-based membranes with ion selectivity for boosting electrochemical energy storage and conversion. *J Mater Chem* 2021;9:25325-40. [DOI](#)
 183. Sheng L, Wang Q, Liu X, et al. Suppressing electrolyte-lithium metal reactivity via Li⁺-desolvation in uniform nano-porous separator. *Nat Commun* 2022;13:172. [DOI](#) [PubMed](#) [PMC](#)
 184. Li C, Liu S, Shi C, et al. Two-dimensional molecular brush-functionalized porous bilayer composite separators toward ultrastable high-current density lithium metal anodes. *Nat Commun* 2019;10:1363. [DOI](#) [PubMed](#) [PMC](#)
 185. Liu Y, Liu Q, Xin L, et al. Making Li-metal electrodes rechargeable by controlling the dendrite growth direction. *Nat Energy* 2017;2. [DOI](#)
 186. Liu K, Zhuo D, Lee HW, et al. Extending the life of lithium-based rechargeable batteries by reaction of lithium dendrites with a novel silica nanoparticle sandwiched separator. *Adv Mater* 2017;29:1603987. [DOI](#) [PubMed](#)